NASA/TM-2000-209710

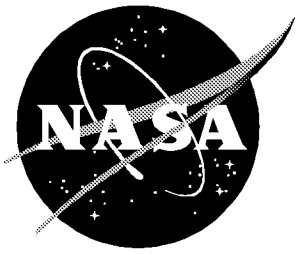

Raman Shifting a Tunable ArF Excimer Laser to Wavelengths of 190 to 240 nm With a Forced Convection Raman Cell

R. Jeffrey Balla and G. C. Herring
Langley Research Center, Hampton, Virginia

April 2000

The NASA STI Program Office . . . in Profile

Since its founding, NASA has been dedicated to the advancement of aeronautics and space science. The NASA Scientific and Technical Information (STI) Program Office plays a key part in helping NASA maintain this important role.

The NASA STI Program Office is operated by Langley Research Center, the lead center for NASA's scientific and technical information. The NASA STI Program Office provides access to the NASA STI Database, the largest collection of aeronautical and space science STI in the world. The Program Office is also NASA's institutional mechanism for disseminating the results of its research and development activities. These results are published by NASA in the NASA STI Report Series, which includes the following report types:

- TECHNICAL PUBLICATION. Reports of completed research or a major significant phase of research that present the results of NASA programs and include extensive data or theoretical analysis. Includes compilations of significant scientific and technical data and information deemed to be of continuing reference value. NASA counterpart of peer-reviewed formal professional papers, but having less stringent limitations on manuscript length and extent of graphic presentations.

- TECHNICAL MEMORANDUM. Scientific and technical findings that are preliminary or of specialized interest, e.g., quick release reports, working papers, and bibliographies that contain minimal annotation. Does not contain extensive analysis.

- CONTRACTOR REPORT. Scientific and technical findings by NASA-sponsored contractors and grantees.

- CONFERENCE PUBLICATION. Collected papers from scientific and technical conferences, symposia, seminars, or other meetings sponsored or co-sponsored by NASA.

- SPECIAL PUBLICATION. Scientific, technical, or historical information from NASA programs, projects, and missions, often concerned with subjects having substantial public interest.

- TECHNICAL TRANSLATION. English-language translations of foreign scientific and technical material pertinent to NASA's mission.

Specialized services that complement the STI Program Office's diverse offerings include creating custom thesauri, building customized databases, organizing and publishing research results . . . even providing videos.

For more information about the NASA STI Program Office, see the following:

- Access the NASA STI Program Home Page at ***http://www.sti.nasa.gov***

- Email your question via the Internet to help@sti.nasa.gov

- Fax your question to the NASA STI Help Desk at (301) 621-0134

- Telephone the NASA STI Help Desk at (301) 621-0390

- Write to:
  NASA STI Help Desk
  NASA Center for AeroSpace Information
  7121 Standard Drive
  Hanover, MD 21076-1320

NASA/TM-2000-209710

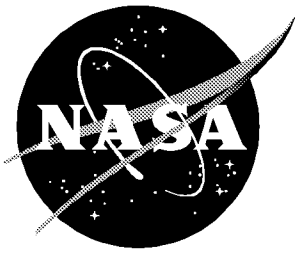

Raman Shifting a Tunable ArF Excimer Laser to Wavelengths of 190 to 240 nm With a Forced Convection Raman Cell

R. Jeffrey Balla and G. C. Herring
Langley Research Center, Hampton, Virginia

National Aeronautics and
Space Administration

Langley Research Center
Hampton, Virginia 23681-2199

April 2000

Acknowledgments

The authors acknowledge technical contributions from B. W. Barnes, R. W. Gregory, Dr. E. Koker, and L. Wade.

Available from:

NASA Center for AeroSpace Information (CASI)
7121 Standard Drive
Hanover, MD 21076-1320
(301) 621-0390

National Technical Information Service (NTIS)
5285 Port Royal Road
Springfield, VA 22161-2171
(703) 605-6000

Abstract

Tunable radiation, at ultraviolet wavelengths, is produced by Raman shifting a modified 285-mJ ArF excimer laser. Multiple Stokes outputs are observed in H_2, CH_4, D_2, N_2, SF_6, *and* CF_4 *(20, 22, 53, 21, 2.1, and 0.35 percent, respectively). Numbers in parentheses are the first Stokes energy conversion efficiencies. We can access 70 percent of the frequency range 42 000–52 000* cm^{-1} *(190–240 nm) with Stokes energies that vary from 0.2* μJ *to 58 mJ inside the Raman cell. By using 110 mJ of pump energy and* D_2, *the tunable first Stokes energy varies over the 29–58 mJ range as the wavelength is tuned over the 204–206 nm range. Dependence on input energy, gas pressure,* He *mixture fraction, and circulation of the gas in the forced convection Raman cell is discussed. Stokes conversion is also discussed for laser repetition rates from 1 to 100 Hz. An empirical equation is given to determine whether forced convection can improve outputs for a given repetition rate.*

1. Introduction

Molecules such as H_2, O_2, N_2, NO, N_2O, H_2O, CO, and CO_2 have spectroscopic transitions in the region from 190 to 240 nm (ref. 1). These molecules are important for many processes, which include combustion chemistry, atmospheric chemistry, and high-speed wind tunnel testing. For example, we are interested in developing diagnostics for O_2 because many wind tunnels use air, and N_2 is more difficult to detect than O_2.

A variety (refs. 2 to 5) of methods for the generation of laser beams in the far ultraviolet (UV) at 200 to 250 nm and vacuum UV (VUV) at ≤200 nm have been pursued. Stimulated Raman scattering (SRS) from an ArF laser is one (refs. 6 to 8) of many approaches. To avoid the disadvantages of multiple lasers, a single laser solution is desirable. Thus, we studied SRS in a forced convection Raman cell (FCRC), which is pumped by a tunable 285-mJ ArF laser. The laser was modified to produce 220 times the spectral brightness of the original commercially available system. Additional excimer-based studies of SRS in H_2 isotopes are in reference 9. Most previous ArF studies used bandwidths ≥1 cm^{-1} and pump energies <100 mJ in static Raman cells. A localized gas flow to replenish gas near the focal volume was previously used in reference 10.

The approach in this paper is oriented towards Stokes production and has several advantages. First, it offers a passive and single-laser method for generating tunable coherent radiation at frequencies outside the laser gain profile. Second, because the Raman gain coefficient increases linearly with increasing pump laser frequency, ArF pumping is enhanced compared with lower frequency sources. Third, ArF pulse energy is high compared with many other laser sources. Last, in specific conditions in some gases, SRS perturbs the gas medium and reduces conversion efficiency on successive pulses. To maintain conversion, the gas medium along the entire length of interaction with the laser beam was replenished between pulses with a commercially available FCRC. The FCRC uses an internal fan to circulate continuously the gas medium transverse to the laser beam propagation direction. This circulation allows improvement of the SRS conversion at higher repetition rates. Short test times (typically 1 to 60 s) in high-speed wind tunnels combined with high run-time costs often dictate a high-repetition-rate laser. This approach also has disadvantages. ArF laser tunability is limited to approximately 300 cm^{-1}. Hence, multiple Stokes shifts in several gases will be required to access a wide frequency range. Generally, excimer-based Raman beam spatial profiles are poorer than YAG-based profiles. Also, absorption of ArF radiation is a problem in many gases.

In this work, the conditions producing optimal SRS are determined empirically by studying conversion efficiency versus relevant parameters for stimulated vibrational Raman scattering (SVRS) and stimulated pure rotational Raman scattering (SRRS) in H_2, D_2, CH_4, N_2, SF_6, and CF_4 at room temperature. The largest tunable Stokes pulse energy of 58 mJ (before exiting the cell), obtained near 205 nm, is

larger than that achieved in earlier studies (refs. 7 and 11). SRS conversion efficiency versus laser repetition rate is measured from 1 to 100 Hz. Results are obtained with and without the FCRC and include an empirical rule to determine when forced convection will be helpful.

2. Stimulated Raman Scattering

When a plane wave of intensity I_p and frequency ν_p (pump wave) traverses a Raman active medium parallel to the x-axis, a fraction of the intensity at ν_p is converted to a copropagating wave at frequency ν_s (Stokes wave) through the Raman scattering process. The conversion of pump wave to Stokes wave is described by (ref. 12)

$$I_o = I_i \exp(gI_pL) \tag{1}$$

where I_i is the initial Stokes intensity (J/sec-m^2) at $x = 0$ and I_o is the amplified Stokes intensity at $x = L$ after traversing a distance L. If the product gI_pL is $\ll 1$, then equation (1) reduces to

$$I_o - I_i = I_i g I_p L \tag{2}$$

In this limit, the generated Stokes intensity, $I_o - I_i$, is linearly dependent on I_p and is determined from the product of two different intensities, I_i and I_p. The plane-wave, steady-state Raman gain coefficient g (m/W) (ref. 9) is

$$g = \frac{2\lambda_s^2 \, \Delta N}{h\nu_s \pi \, \Delta\nu} \frac{d\sigma}{d\Omega} \tag{3}$$

where λ_s is the Stokes wavelength, $\Delta\nu$ is the full width at half maximum (FWHM) Raman bandwidth, $d\sigma/d\Omega$ is the differential Raman cross section for the chosen Raman transition, polarization, and scattering direction. The population difference between the initial and the final levels is ΔN. Usually v and J denote vibrational and rotational quantum numbers. Since $d\sigma/d\Omega$ varies as ν^4, g varies as ν; hence g is enhanced for the ArF laser compared with all lower frequency light sources.

If a second wave at the Stokes frequency ν_s is also injected with the pump wave such that it copropagates with the pump, then this second wave will act as the seed I_i for the conversion process. In Raman shifting, we are interested in one-laser configurations where only the pump wave at ν_p initially enters the Raman medium. Then the initial Stokes intensity I_i originates from spontaneous Raman scattering that occurs in a small solid angle centered on the forward direction. Equation (1) can still be used to calculate the conversion to the Stokes frequency if the strength of the spontaneous Raman scattering can be estimated.

Equations (1) to (3) describe conversion for an ideal plane wave, but are not adequate for accurate calculations in the more practical case of a focused Gaussian-shaped laser beam. For Gaussian beams, one can integrate over the focal region to get (refs. 9 and 12)

$$P_o = P_i \exp\left[\frac{4gP_p \arctan(L/b)}{\lambda_p + \lambda_s}\right] \tag{4}$$

where b is the confocal parameter, λ_p is the wavelength of the pump beam, P_i and P_o are the powers (J/s) of the Stokes beam at $x = 0$ and $x = L$, respectively, and P_p is the pump beam power.

Equations (1) and (4) illustrate how the generation of Stokes light is nonlinearly dependent on I_p or P_p. This Raman conversion to Stokes energy also exhibits a threshold behavior. As the pump intensity is increased from very small values, one observes relatively little conversion to the Stokes wavelength. Near the threshold intensity, $I_p = I_{th}$, the conversion dramatically increases as I_p increases only slightly. Finally, the fraction of light converted becomes roughly constant as I_p is increased further. Most of the conversion occurs over a small range of pump intensities near I_{th}. For a focused Gaussian beam in a Raman medium much longer than the confocal parameter, the pump beam power P_{th} needed to achieve threshold for the Raman process is (refs. 9 and 13)

$$P_{th} = \frac{25\lambda_p}{\pi g} \tag{5}$$

Threshold is defined as the pump power necessary to obtain $P_o/P_i = \exp(25)$ in equation (4). This empirical definition is based on a variety of experimental observations. The ratio P_o/P_i represents the total integrated gain through the focal region. This gain is sometimes expressed in nepers (Np). One Np is defined as a gain of exp(1), thus $\exp(25) = e^{25} = 25$ Np.

3. Experiment

3.1. ArF Excimer Laser Configuration

A schematic diagram of the experiment is shown in figure 1. The pump laser consists of a modified Lambda Physik model LPX250T pulsed, dual-discharge tube tunable ArF excimer laser. A detailed description of the characteristics and modifications of this design has been presented in reference 14. This design has a bandwidth of 0.33 cm^{-1}, a FWHM pulse of 15 ns, peak locking efficiency of 98 percent, and tunability from 51570 to 51870 cm^{-1} with >30-percent locking efficiency. The output beam is 8 mm high by 10 mm wide, diverges nine times the diffraction limit of a 10-mm-diameter Gaussian beam, and has a horizontal-to-vertical polarization ratio of 35:1. Overall, spectral brightness is increased 2 orders of magnitude when compared with the standard unstable-resonator amplifier design. With new discharge tube windows, the output is 285 mJ. As the MgF_2 windows absorb water and become dirty, the output can significantly decrease.

All optics (outside the laser) in figure 1 are uncoated Heraeus Amersil Suprasil quartz with focal lengths specified for 193-nm radiation. Those between the laser output and center of the FCRC transmit 70 percent, giving a pump energy of 200 mJ inside the cell if the laser produces 285 mJ. The beamsplitter before the FCRC diverted a fraction of the backward stimulated Brillouin scattering (SBS) and backward SRS. These were measured following dispersion by a prism. The optics on the output side of the FCRC also transmitted about 70 percent of the output Stokes wavelengths. Thus usable pulse energies after the final dispersing prism are about 70 percent of what is generated inside the cell.

3.2. Forced Convection Raman Cell

The FCRC consists of a closed Raman cell with an internal fan to circulate continuously the gas medium transverse to the laser beam propagation direction. It removes or dilutes the gas medium that has been perturbed by SRS on prior laser pulses. This device is available commercially from Light Age, Inc. Using the manufacturer's lens or window thickness of 0.95 cm, the maximum recommended operating density was 157 amagats (2500 psi at 296 K). Densities are specified in amagats, where 1 amagat is the density of an ideal gas at standard temperature and density (273.15 K and 1 atm). The FCRC contains an internal variable-speed fan with four blades. Each blade extends outward 0.95 cm from the main shaft. The shaft and blades run parallel to the laser beam, span the length of the FCRC, and circulate the gas transverse to the laser beam. A 0–24 V DC (direct-current) motor drives the fan. Fan tip rotation was measured at atmospheric density and was found to be linear with applied voltage. The maximum of 24 V corresponds to 100 rps and a fan tip speed of 600 cm/s, but only at 1 atmosphere.

All gases were research grade purity except D_2 (99.7+ percent), CF_4 (99.97 percent), and SF_6 (99.999 percent). The gases in the following table with the manufacturer's stated minimum purities were used:

Gas	Minimum purity, percent
H_2	99.9999
D_2	99.7+
CH_4	99.995
CF_4	99.97
SF_6	99.999
N_2	99.9995
He	99.9999

Several cell geometries were used to vary confocal parameter. The first, in figure 1, uses a lens (2 in. diameter by 65 cm focal length) to reduce the beam diameter before entering the FCRC input window (12 mm diameter). This eases alignment difficulties and focuses more energy into the cell than an integrated (i.e., a lens also acting as the Raman cell window) optic. A second geometry used a 1-m long cell with integrated optics (50-cm focal length). A third geometry combined 0.5 and 1.0 m FCRC's to produce a single cell (with two internal fans) with a length of 1.5 m and integrated optics (80-cm focal length). The FCRC window-seal design required densities above 1.2 amagats to maintain gas seal integrity.

3.3. Optimization of SRS

Output Raman energy was studied as a function of several parameters:

(1) Pump-laser beam focal length

(2) Raman cell gas density

(3) Pump-laser energy

(4) Helium mixture fraction

(5) FCRC fan voltage (i.e., fan speed, rps)

(6) Pump-laser pulse repetition rate

Energy measurements were made of the incident pump, transmitted pump Q_0, first SVRS Stokes order Q_1, and higher Stokes orders Q_n. Surrounding each Q_n, a series of equally spaced SRRS transitions on both the high and low frequency side was observed. SRRS transitions on the lower frequency side are designated $Q_{n,+1}$, $Q_{n,+2}$, $Q_{n,+3}$, ..., whereas those on the higher frequency side are designated $Q_{n,-1}$, $Q_{n,-2}$, $Q_{n,-3}$, ... With this notation, the first Stokes pure rotational shift is $Q_{0,+1}$, the second Stokes pure vibrational shift is Q_2, and the third anti-Stokes rotational shift off the first Stokes vibrational shift is denoted by $Q_{1,-3}$. Multiple detectors were used to verify detector calibrations. These detectors included both pyroelectric (Molectron J4-09, Laser Precision model RJP-735-RO, and Coherent model LMP10) and calorimeter energy meters (Coherent model LM100E and Scientech Model 380103). All detectors agreed within 10 percent over the appropriate energy ranges. Single pulse spatial profiles of selected beams were captured with a CCD camera.

Typically, 50 to 90 percent energy conversion was observed into the sum of all Stokes transitions. Anti-Stokes production occurs at VUV frequencies. No attempt was made to measure vibrational anti-Stokes yields, where the room air and optics strongly absorb radiation below 190 nm. The few anti-Stokes transitions observed were pure rotational shifts with wavelengths above 190 nm.

4. Results

When a high-intensity laser is focused into a gas, SRS and four-wave mixing (FWM) occur (ref. 15) simultaneously. The first is cascade SRS where Q_n becomes intense enough to generate Q_{n+1}. SRS exhibits a threshold behavior; that is, at a specific input Q_n intensity, the conversion to Stokes light Q_{n+1} dramatically increases in a nonlinear manner. The second process is FWM using four consecutive Q_n orders. FWM processes have no threshold but do require phase matching. Cascade SRS tends to dominate the production of low order ($n = 1,2$) Q_n and FWM tends to dominate the production of higher orders ($n \geq 3$) (ref. 7).

To maximize the energy in Q_1 or Q_2, FWM should be minimized. FWM can be reduced by two methods (ref. 16). Large densities will prohibit phase matching in the forward direction, whereas long focal lengths eliminate off-axis propagation angles that satisfy the phase-matching condition in the near-forward direction.

The pump-beam focusing was primarily constrained by the FCRC length. A focal length too short requires a collimating lens internal to the cell, and one too long may burn the cell windows. We measured conversion in H_2 and N_2 for 50- and 65-cm focal lengths at 193 nm. We used pump energies above 50 mJ because this study seeks maximum output energies, not high conversion efficiency. Below 10 amagats, Q_1 and SRRS transitions are larger with the 65-cm focal length. Above 10 amagats, Q_2 generally dominates the output spectrum. Conversions for $Q_1 - Q_3$ vary less than 25 percent for the two focal lengths. Unless stated otherwise, a 65-cm focal length was used for this work; the few times that a 50-cm lens was used are clearly stated. Optimum energy production into any desired order is achieved by varying density.

The following conditions apply to all results unless stated otherwise. Absolute energy measurements were made of the incident pump energy, the residual pump energy Q_0, and SRS energy in all observed Stokes orders. All conversion efficiencies and all pulse energies for the transmitted pump Q_0 and Stokes beams are values inside the FCRC after correction for transmission losses of 30 percent exiting the cell. Since the input optics of the Raman cell also attenuate the pump energy by 30 percent, pump energy values listed on the x-axis of the figures in this report have been reduced by 30 percent to give energy values inside the Raman cell. Conversion efficiencies are listed as percent energy conversions inside the cell. All experiments were performed at 296 K. Those that varied pump energy, confocal parameter, He mixture

fraction, or gas density are performed at 10 Hz with a 1-m-long FCRC operating at 24 V on the fan motor. All experiments, except the few times that the laser was scanned, are performed with the laser tuned to 51714 cm^{-1}.

4.1. H_2

The vibrational Raman shift of H_2 is 4155.3 cm^{-1} (ref. 17). Stokes Q-branch conversion versus H_2 density is shown in figure 2 using 83 mJ of pump. Although not shown in the figure, the Stokes outputs remain constant at the 60-amagat values out to 100 amagats. Attempts were made to optimize Q_1 at pump energies above 100 mJ by adding 50-amagat helium or argon (refs. 16 and 18) to 50-amagat H_2. Energy conversions $Q_1 - Q_3$ were unaffected by these additions. Addition of 6-amagat N_2 to 50-amagat H_2 increased Q_1 conversion by 20 percent at the expense of $Q_2 - Q_3$. Energy conversion $Q_1 - Q_3$ versus pump energy is shown in figure 3 for 20-amagat pure H_2. Experiments performed with the FCRC fan on and off show no measurable effect on any $Q_1 - Q_3$ over a range of 10- to 30-Hz repetition rates.

At H_2 densities <6 amagats, a series of transitions were observed surrounding each Q_n transition, and this is shown in figure 4. To determine if these Raman orders are pure rotational ($\Delta J = 2$) or O and S branch rotational-vibrational transitions, we accurately measured the wavelengths. For any Q_n, the frequency difference between Q_0 and $Q_{0,1}$, Q_1 and $Q_{1,1}$, Q_2 and $Q_{2,1}$ was measured to be 587.0 ± 0.3 cm^{-1}, where the uncertainty of ± 0.3 cm^{-1} is estimated from the variation of repeated measurements. This frequency difference corresponds to $\Delta J = 2$, for $J = 1$ to 3. The transition is known to be 587.0 cm^{-1} (ref. 19). Thus these transitions correspond to pure rotational Raman shifting. They are referred to as SRRS transitions and labeled $Q_{n,\pm m}$, where n refers to the vibrational order and $\pm m$ refers to the rotational order.

Conversions versus pump energy for SRRS transitions are shown in figure 5. Conversions versus H_2 density are shown in figure 6. Above 6 amagats, only Q_n transitions are observed, whereas the SRRS orders disappear. Note that >90 percent of the pump energy is converted into forward Stokes orders under some conditions.

4.2. CH_4

The vibrational Raman shift corresponding to the ν_1 transition is 2916.5 cm^{-1} (refs. 20 and 21). SRS in static CH_4 with high UV intensities generally results in multiphoton decomposition or breakdown (ref. 22). We minimized this problem by flowing the CH_4. Figure 7 shows CH_4 SRS in a closed FCRC, which produced a rapid temporal decay in conversion. The transmitted pump laser energy decreased 30 percent during the experiment. Results identical to figure 7 were obtained four successive times by refilling the FCRC. Results were independent of fan on or off. Removal and examination of the FCRC windows following all four runs indicated they were unaffected by the window-soot problem sometimes encountered (ref. 23). Results suggest a process creating photochemical decomposition whose products absorb ArF radiation. To overcome this problem, the laser entrance end of the FCRC was opened to the CH_4 cylinder while a mass flow controller was attached to the other end. The results obtained are shown in figure 7 with a flow of 6 SLM (standard liters per minute) of CH_4. All results in pure CH_4 and CH_4-He mixtures were acquired with this flowing Raman medium. After 2 to 3 days of work, a round black spot coincident with the pump beam appeared on the FCRC input window. The transmitted pump beam energy decreased by 30 percent. The window was readily cleaned with methanol.

Above 7 amagats, Q_1 and Q_2 conversions were the same for the 65- and 50-cm lenses; therefore, the 65-cm lens was used to acquire all further CH_4 data. Conversions versus CH_4 density are shown in figure 8 and are independent of fan on compared with fan off at ≤10 Hz. As with H_2, Q_2 exceeds Q_1 as density increases.

Helium addition (ref. 24) can vary the competition between backward SBS and SRS in a CH_4-He mixture and forward SRS. Results of backward and forward SRS versus He density are shown in figure 9. The backward SBS signal could not be distinguished from scattered pump laser in the case of CH_4. The maximum backward Q_1 signal, measured to be 1 μJ, was swamped by back-scattered pump. To remove the latter, backward Q_1 was observed by using a photomultiplier tube (PMT) after passage through a 1/4-m monochromator. Relative values obtained versus He

were normalized to the 1-μJ signal levels, then corrected for transmission losses to calculate conversions inside the FCRC. This method provides an order-of-magnitude estimate of backward Q_1. Forward Q_1 increases slightly at the expense of forward Q_2 and backward Q_1, as the He partial density is increased.

Conversion versus pump energy is shown in figure 10; Q_2 exceeds Q_1 at 50 mJ and both exceed Q_0. As with H_2, the FCRC has no measurable effect on conversion under these conditions.

4.3. D_2

The vibrational Raman shift of D_2 is 2987.3 cm^{-1} (ref. 25). No experiments were performed to study conversion in D_2 versus focal length. Results similar to H_2 are expected. Q-branch conversion versus D_2 density is shown in figure 11. Above 4 amagats, Stokes lines greater than Q_3 decrease with increasing D_2 density indicating FWM effects. Like H_2, $Q_1 - Q_3$ conversion is independent of density above 5 amagats. Energy conversion $Q_1 - Q_4$ at 26-amagat D_2 versus pump energy is shown in figure 12; Q_2 exceeds Q_1 above 65 mJ, but unlike H_2 and CH_4, neither exceeds Q_0.

At pump energies above 50 mJ and densities from 1 to 10 amagats, rotational transitions surrounding the expected Q_n vibrational transitions were observed in D_2 similar to those observed in H_2. The frequency spacing is measured as 408 ± 11 (±1σ) cm^{-1}. This spacing corresponds to transitions between $J = 2$ and 4. The rotational Raman shift corresponding to the $S(2)$ transition is 414.6 cm^{-1} (ref. 25). By analogy with H_2, these transitions are the result of cascade pure SRRS. Conversion versus pump energy is shown in figure 13 for transitions near Q_0 and Q_1. Conversion versus D_2 density is shown in figure 14. Unlike H_2, D_2 transitions require higher pump energies and generate fewer SRRS transitions. Like H_2, they have similar conversions and occur over similar density ranges. At 1.2 amagats, only transitions surrounding Q_0 and Q_1 were observed, with 53 percent conversion into Q_1. Small density changes in the range of 1 to 5 amagats change significantly the conversions observed in various orders. As with H_2 and CH_4, the FCRC has no measurable effect on conversion.

As in H_2, results show an optimal density for conversion into a given transition. Also, as in H_2, low densities (1 to 3 amagats) optimize pure rotational transitions and Q_1. Moderate densities (3 to 5 amagats) optimize Stokes above Q_3. High densities (>5 amagats) optimize Q_2 and Q_3. Note that the intensity of our pump laser is large enough that we easily observe SRRS for H_2 and D_2 at 296 K.

4.4. N_2

The vibrational Raman shift is 2329.9 cm^{-1} (ref. 26). The FCRC affects SRS significantly in N_2. Results showing conversion versus N_2 density with the FCRC fan on and off are presented in figure 15. The fan-off condition versus time caused the location of the laser beam on the FCRC output window to fluctuate from pulse to pulse. The beam also increases in size and overfills the FCRC output window because of thermal self-actions in the static gas as discussed in sections 4.8 and 5.1. In this case, accurate conversions could not be measured. The measured output energies with the fan off (and the cell clipping the beam) are shown for comparison. At 89 amagats, the fan-on condition improves measured output energy by a factor of approximately 300. At intensities less than 1 percent of Q_1, Q_2 was observed intermittently. Most N_2 data were acquired with a fan voltage of 24 V. Reducing the fan voltage from 24 V to 10 V could decrease conversion by 25 percent.

Conversions at 95-amagat N_2 were measured versus time for fan-on and fan-off conditions. For fan off, temporal decays similar to those of CH_4 were obtained. With the fan off at Time = 0, a 5-shot average at 10 Hz produced 8 percent conversion. After 30 s at 10 Hz with fan off, conversion decreased by a factor of 20. This decay was reproduced after running the fan for a minute or waiting 15 min with the fan off. Successive laser pulses build up the vibrational excitation but do not destroy the N_2 medium.

Previous work (ref. 27) used relatively long focal lengths for Raman shifting in O_2. For N_2, similar to O_2, we first determined that the 65-cm lens gave 25 percent more conversion than the 50-cm lens. All other N_2 results were acquired by using the 65-cm lens and the 1.5-m FCRC. Results in pure N_2 and two N_2-He mixtures are shown in figure 16. N_2 partial densities are listed on the abscissa. To ensure uniform composition, the FCRC circulated each mixture for at least 4 hr and the mixture stood overnight. Next, a

series of measurements were obtained by decreasing the total pressure.

Results of backward SRS and SBS versus added He density are shown in figure 17. In pure N_2, backward and forward SRS conversions are comparable. He addition reduces backward SRS and SBS while increasing forward SRS.

Energy conversion Q_1 was measured versus pump energy (18 to 100 mJ) for a 7:1 N_2-He mixture (Total density = 126 amagats). Unlike H_2, CH_4, and D_2, Q_1 conversion in N_2 remains approximately constant. Energy conversion Q_1 decreases by only 20 percent as the pump varies from 40 to 18 mJ. Above pump energies of 40 mJ, Q_1 conversion was constant.

4.5. SF_6 and CF_4

The prominent ν_1 SF_6 vibrational Raman transition is shifted 774.5 cm^{-1} (refs. 21 and 28). Conversions in SF_6 are low and difficult to obtain. Conversions of both Q_1 and Q_2 could not be maintained above 4 Hz. Most experiments were performed at 3 Hz. None were performed as a function of focal length. Conversion in pure SF_6 was optimal at pressures near the SF_6 condensation point (≈20 amagats in the nonshaded part of fig. 18) and when fan speeds were minimal. The fan motor was powered with 8 V. Helium addition produced results similar to CH_4 and N_2 as shown in the shaded part of figure 18. At the curve peak in the shaded part of figure 18, Q_3, Q_4, and Q_{-1} were observed, all three with conversions of about 0.003 percent. No backward SRS or SBS experiments were performed.

Conversions in the optimal SF_6-He mixture in the shaded part of figure 18 were independent of pump energy from 15 to 60 mJ. With the FCRC fan off and using the optimum SF_6-He mixture, results similar to CH_4 and N_2 were observed. Conversions decreased by 1 order of magnitude after 10 min at 1 Hz in a closed cell with the fan off.

The vibrational Raman shift in CF_4 of the ν_1 transition is 909.1 cm^{-1} (refs. 21 and 29). Results are similar to SF_6. Conversions in pure CF_4 and CF_4-He mixtures are presented in table 1. Helium addition produced results similar to CH_4, N_2, and SF_6. Conversions Q_3, Q_4, and Q_{-1} were generated as rings, which suggests they were due to FWM. Like SF_6, conversion was optimal when fan speeds were minimal (8 V) and could not be maintained above 4 Hz. No backward SRS, SBS, or further studies were performed due to the low conversions.

Low conversions in these two gases have several reasons. First, the Raman gain coefficients are small. Second, competition with backward SRS and SBS (ref. 30) reduces the forward Raman. Third, without a FCRC there are severe prior-pulse effects. Using a FCRC, along with He addition, reduces the magnitude of this problem. Fourth, SRS is observed only near the liquefaction point; this combined with high fan speeds created refractive index gradients, which were observed visually in the FCRC. Their intensity increased with fan speed, which precluded the use of relatively large fan speeds for these two gases. However, some finite fan speed is necessary to get any increase in the heat dissipation. These two ideas are consistent with our observation of optimal conversion at one particular relatively low fan speed.

4.6. Spatial Profiles of Raman Shifted Beams

Figure 19(a) shows 25 pulse averages for the first four Stokes orders after Raman shifting in pure CH_4. These images were captured on a video camera. Figure 19(b) shows four different single pulse images for the first Stokes, and figure 19(c) shows four single pulse profiles for the fourth Stokes. These pure CH_4 results are typical of most of our spatial profiles.

Raman shifting in H_2, D_2, and CH_4-He mixtures generally gave better spatial profiles than those of pure CH_4 in figure 19. Large gain coefficients (i.e., well above threshold) and efficient thermal conduction for these cases help to give better spatial profiles. By better, we mean more circularly symmetric than those of figures 19(b) and 19(c). Conversely, Raman shifting in CF_4, SF_6, and N_2 (all three mixed with He) consistently gave poorer spatial profiles (i.e., unsymmetric patterns with random hot spots) than those of figure 19. These poorer spatial profiles occur because of the relatively small gain coefficients (i.e., closer to threshold) and poorer thermal conductivity. Pure N_2 profiles were the worst, showing filamentary-type intensity distributions (ref. 31) that are characteristic of self-focusing or self-trapping.

4.7. Accessible Frequency Range

Table 2 lists the accessible frequency range for each Raman transition of each gas, along with the maximum conversion efficiencies obtained at the center of each range. Combined, they cover approximately 70 percent of the frequency range from 42 000 to 52 000 cm^{-1}. The endpoints of the tuning ranges are defined to be where the locking efficiency of the laser drops to 30 percent. At both endpoints, the Stokes output pulse energies typically fall to about one half maximum because the laser energy and the locking efficiency both decrease as it is tuned off of the center frequency. We observe only minor variation in conversion efficiency above 40 mJ of input pump energy in most gases, and keeping the laser energy above 150 mJ is very time-consuming. Thus the results in table 2 were acquired over a wide range (40–170 mJ inside the cell) of pump energies. The Stokes energies corresponding to the conversion efficiencies in table 2 vary from 0.2 μJ to 58 mJ, depending on the input pump energy, gas, and Stokes transition. One result, using 110 mJ of pump energy and D_2, is a conversion efficiency of 53 percent and a tunable Stokes energy that varies over the range of 29 to 58 mJ as the first Stokes wavelength is tuned over the range of 204 to 206 nm. We anticipate increasing these Stokes energies by about a factor of 2 by using the full pump energy and MgF optics in the cell.

4.8. Laser Pulse Repetition Rate

Stokes conversion, input pump energy, and residual pump energy versus laser repetition rate are shown for H_2, CH_4, D_2, N_2, and SF_6 in figures 20 through 25. Figure 21 differs from figure 20 by the pump energy that is used. For the first Stokes of H_2 and D_2, forced convection does not make any difference, even at a pulse rate of 100 Hz. Higher Stokes orders are helped by the circulation of the gas. In CH_4, in spite of the pressure-induced flow from the CH_4 bottle, the fan-induced motion helps Raman conversion at >10 Hz. For N_2, SF_6, and CF_4, using forced convection (i.e., fan on) improves the conversion at higher repetition rates compared with fan off. At rates as low as 1 Hz, for these 3 gases, circulation of the gas is necessary to get any consistent output.

In many gases, we observe a 10- to 20-percent increase in Q_1 and Q_2 conversion as the repetition rate varies from 10 to 100 Hz. This increase occurs because the ArF laser cannot maintain pulse energies above 50 Hz. The input pump energies are plotted with the right-hand axes. The decreasing pump energy eventually drops below threshold for the higher orders; this makes more pump energy available for conversion into the lower orders, which are still above threshold. This results in the increase, versus repetition rate, of the low orders in figures 20 to 25.

Without exchanging the gas between laser shots, N_2 SRS is limited to very low (<1 Hz) repetition rates, where mass and thermal diffusion can maintain equilibrium. Pure N_2 has a relatively long vibrational lifetime for $v = 1$. At 298 K, reference 32 quotes a lower limit of >1 atm-s. We estimate 3×10^3 atm-s, which is based on high temperature data (ref. 33). The N_2 lifetime at 157 amagats (170 atm) is estimated to be 18 s. Successive pulses at 10 Hz would create significant population in $v = 1$ and reduce conversion.

Helium (ref. 32) was added to N_2 to increase the vibrational relaxation rate. However, in static conditions (i.e., no fan), good conversion was still limited to low repetition rates. High conversion for the first 5 to 10 pulses suggests that gas breakdown is not the problem. But observations of fluctuations in beam size and location on the output FCRC window indicate that thermal "lensing" is a problem. Using the fan did eliminate these effects and improve the output beam profile and reduce the motion. Figure 24 shows that the fan allows reasonable conversion at repetition rates up to 10 Hz.

4.9. Raman Threshold Power Measurements

Our best threshold measurement is in H_2 at 4 amagats. Using 1.5 mJ of pump, 18 percent conversion into Q_1 is observed without any higher Stokes orders. Decreasing the pump energy to 0.75 mJ produced no Q_1. Thus we estimate an experimental threshold power of 1 mJ/15 ns ≈ 70 ± 30 kW for our apparatus. This estimate is about 8 times larger than the calculated value of 8 kW from equation (5).

We also measured threshold for N_2, although less reliably than for H_2. For 146 amagats of pure N_2, we see minimal Stokes production with 12 mJ of pump. Visual inspection of the beam suggested that we were close to threshold; however, we did not decrease the

power to watch the Raman conversion disappear because we were not interested in threshold powers at the time. Thus $P_{th} \leq 12$ mJ/15 ns ≈ 0.8 MW. The calculation with equation (5) is 95 kW. As in the measurement of H_2, the N_2 upper limit is ≈8 to 9 times larger than expected for an ideal focused Gaussian beam.

This disagreement is reasonable, since our pump beam is ≈9 times worse than the diffraction limit (section 3.1). Hence we expect that the pump beam will not focus as tight as possible and that the threshold will be raised above the expected value of $e^{25} = 25$ Np for near diffraction limited beams. Since we observe threshold at $9 \approx e^2$ times the value predicted by equation (5), we are observing threshold at about $e^2 e^{25} = 27$ Np for both H_2 and N_2.

Similar to N_2, we also obtained an upper limit of threshold for SF_6. For a 1:1 mixture of SF_6-He at a total density of 29 amagats, P_{th} is less than or equal to 0.47 MW for SF_6.

5. Discussion

5.1. Limitations for Raman Conversion

The SRS process perturbs a gas medium in a variety of ways (refs. 34 and 35) that can reduce conversion efficiency. A few of these processes are discussed. First, for each Stokes photon produced, a molecule is excited to $v = 1$. But conversion efficiency depends on the population difference. If these excited molecules do not return to $v = 0$ between successive pulses, conversion is reduced. Vibrational relaxation lifetimes are listed in table 3. (Data in table 3 are from refs. 36 to 42, 33, and 32.) Even at 100 Hz, relaxation between laser pulses for all gases is complete except in N_2. Second, regardless of the mechanism or rate by which the perturbed medium equilibrates, the final result is energy transfer into translational motion. Hence, significant heat can be deposited in the interaction volume and perturb the propagation of subsequent pulses through the medium. Third, optically induced ionization can destroy the Raman medium. Finally, large laser intensities can nonlinearly perturb the index of refraction to change the beam propagation on the nanosecond time scale of a single pulse. These previous processes are known as saturation, thermal lensing, optical breakdown, and self-focusing, respectively.

These processes can degrade the spatial beam quality, create large fluctuations in the spatial location of the output Raman beam, and prevent the beam from focusing properly. In general, they also reduce conversion in the SRS process. They can occur during a single pulse (transient self-actions) or be the result of a prior pulse or series of pulses (thermal self-actions). The influence of thermally related perturbations is governed by the removal of heat through natural convection and diffusion. Previous researchers (e.g., ref. 24) added He to the gas medium to increase the thermal conductivity.

For N_2, Stokes output beam spatial profiles that are filamentary in nature are observed. This observation suggests that self-focusing is occurring and that the input beam is not uniform. Addition of He to N_2 reduces, but does not eliminate, this beam degradation.

To check for laser-induced breakdown of the gas medium, a second cell (one with a side window but unable to take high pressures) was filled with 1 atm of N_2. With 200 mJ inside the cell, we observed breakdown with a 50-cm focal length lens and no breakdown with 57- and 65-cm lenses. Filling the cell with 1 atm of H_2 again showed no sign of breakdown with the 65-cm lens. Almost all the data presented here were obtained with the 65-cm lens. These tests do not prove that we are avoiding breakdown because the breakdown threshold will be lowered (relative to 1 atm) at the high pressures used for Raman shifting. Unfortunately, there are no side windows on the FCRC to use for visual confirmation of breakdown.

5.2. Increasing the Repetition Rate With a FCRC

In this section, an empirical method is presented for determining repetition rates for which our FCRC will be effective in improving Raman beam output energies or spatial profiles. One method for eliminating prior-pulse effects is to exchange the medium after each laser pulse (not only at the focal volume, but along the entire length of the laser beam). This was demonstrated (ref. 43) with a cw (continuous-wave) laser beam inside a wind tunnel. That work showed

that prior-pulse thermal effects were minimized at velocities near 250 cm/s, and these velocities had negligible effects on beam profile.

The FCRC achieves similar improvements except in a closed system. The nonequilibrium medium is removed or diluted in the surrounding medium, and this provided time to equilibrate. The FCRC will be effective for nonequilibrium whenever the perturbed medium cannot equilibrate between pulses. If vibrational relaxation is assumed complete and no optical breakdown, the problem reduces to heat dissipation. One method for estimating when the FCRC will be effective for heat dissipation is to compare the thermal diffusion length L (ref. 15) with the focused beam diameter D. The diffusion length depends on the pulse repetition rate f as

$$L(f) = \left(\frac{8k}{f\rho C_p}\right)^{1/2} \qquad (6)$$

The density is ρ, the specific heat capacity is C_p, from reference 21, and the thermal conductivity is k, from reference 44 for all gases except SF_6 and CF_4 and from reference 45 for SF_6 and CF_4. For comparison of gases, table 4 shows values of diffusion length $L(10)$ calculated for our Raman cell conditions and a pulse rate of 10 Hz. Table 4 suggests that conversion can be maintained at higher repetition rates for the sequence $SF_6 < N_2 < CH_4 < D_2 < H_2$. Results in figures 20 to 25 are consistent with this suggestion.

Prior-pulse effects should be small when L becomes several times D. To test this idea, calculate $L(f_{1/2})$ at the repetition rate $f_{1/2}$, which is the frequency where the Stokes output has decreased to 50 percent of the low repetition rate value. Table 5 presents the ratio $L(f_{1/2})/D$ for five cases. In each case, we use the lowest Stokes transition that is observed to weaken with increasing frequency. For all transitions listed in table 5, the conversion efficiency is ≥10 percent (except the backward O_2-He mixture case which is 7 percent). This criterion implies that the gain in these various transitions is at similar relatively large levels above threshold. Thus significant heating is taking place in each case. The data for H_2, CH_4, and D_2 come from figures 21 to 23. The O_2-He mixture data for forward and backward scattering are estimated from reference 46. The thermal conductivity for the O_2-He mixture is estimated as ≈0.06 J/m-s-K from reference 47. We believe that the two data points for the two O_2-He mixture cases are less reliable than the pure gas results, because of our crude calculation of the thermal conductivity and the limited data points for conversion versus frequency in reference 47.

The ratio $L(f_{1/2})/D$ is about constant at 4 ± 1 for all entries in table 5. The uncertainty is an estimate simply based on the spread of values in table 5. This implies that $L(f_{1/2})/D \approx 4$ can be used as a rule of thumb to estimate repetition rates where this FCRC will become effective in improving conversion and beam quality. If $L/D < 4$, then the internal fan will help. If $L/D > 4$, natural diffusion and convection will suffice. Our observed value of 4 ± 1 for L/D in gases is similar to the value of 2.7 observed (ref. 15) in liquid nitrogen.

6. Concluding Remarks

We have studied the production of high-pulse-energy tunable laser radiation at far ultraviolet frequencies. This is achieved by combining a high-spectral-brightness tunable 285-mJ ArF excimer laser, stimulated Raman scattering, and a forced convection Raman cell. Multiple stimulated Raman transitions in H_2, CH_4, D_2, N_2, SF_6, and CF_4 are observed. We can access 70 percent of the frequency range from 42000 to 52000 cm^{-1} with a Raman beam energy of ≈60 mJ in the best case of D_2 (first Stokes energy conversion efficiency of 53 percent). Addition of He to the Raman gas greatly improves the conversion in N_2, SF_6, and CF_4. Threshold intensities for vibrational Raman conversion are found to be ≈8 times larger than calculations for ideal Gaussian beams. Pure rotational Raman conversion in H_2 and D_2 is obtained at room temperature.

The vibrational Raman conversion efficiency versus laser repetition rate was measured. Energy conversions of Q_1 and Q_2 in H_2 and Q_1 in D_2 do not decrease from 1 to 100 Hz in a static cell. But, conversions in higher orders of H_2 and D_2 and Q_1 of lower-gain gases (N_2, CH_4, and SF_6) decrease as repetition rate increases due to prior-pulse effects (e.g., heating) on the Raman medium. We show the effectiveness of forced convection to improve Raman conversion at higher repetition rates by circulating the gas inside the Raman cell to decrease these effects. At room temperature, if the thermal diffusion length is less than

≈4 times the focused beam diameter, the FCRC will be useful in increasing conversion efficiencies at higher pulse rates. Using this FCRC, maximum conversion efficiency can be maintained up to 100 Hz in Q_1 of CH_4, 50 Hz in Q_3 of D_2, 20 Hz in Q_2 of CH_4, 10 Hz in Q_1 of N_2-He, and 5 Hz in Q_1 and Q_2 of SF_6-He.

7. References

1. Okabe, Hideo: *Photochemistry of Small Molecules*. John Wiley & Sons, 1978.

2. Heitmann, U.; Kötteritzsch, M.; Heitz, S.; and Hese, A.: Efficient Generation of Tunable VUV Laser Radiation Below 205 nm by SFM in BBO. *Appl. Phys. B*, vol. 55, 1992, pp. 419–423.

3. Strauss, Charlie E. M.; and Funk, David J.: Broadly Tunable Difference-Frequency Generation of VUV Using Two-Photon Resonances in H_2 and Kr. *Opt. Lett.*, vol. 16, no. 15, Aug. 1991, pp. 1192–1194.

4. Cromwell, E.; Trickl, T.; Lee, Y. T.; and Kung, A. H.: Ultranarrow Bandwidth VUV-XUV Laser System. *Rev. Sci. Instrum.*, vol. 60, no. 9, Sept. 1989, pp. 2888–2892.

5. Ludewigt, K.; Pfingsten, W.; Möhlmann, C.; and Wellegehausen, B.: High-Power Vacuum-Ultraviolet Anti-Stokes Raman Laser With Atomic Selenium. *Opt. Lett.*, vol. 12, no. 1, Jan. 1987, pp. 39–41.

6. Dreier, T.; Dreizler, A.; and Wolfrum, J.: The Application of a Raman-Shifted Tunable KrF Excimer Laser for Laser-Induced Fluorescence Combustion Diagnostics. *Appl. Phys. B*, vol. 55, 1992, pp. 381–387.

7. Loree, T. R.; Sze, R. C.; Barker, D. L.; and Scott, P. B.: New Lines in the UV: SRS of Excimer Laser Wavelengths. *IEEE J. Quant. Electron.*, vol. QE-15, no. 5, May 1979, pp. 337–342.

8. Döbele, H. F.; Röwekamp, M.; and Rückle, B.: Amplification of 193 nm Radiation in Argon-Fluoride and Generation of Tunable VUV Radiation by High-Order Anti-Stokes Raman Scattering. *IEEE J. Quant. Electron.*, vol. QE-20, no. 11, Nov. 1984, pp. 1284–1287.

9. Faris, Gregory W.; and Dyer, Mark J.: Raman-Shifting ArF Excimer Laser Radiation for Vacuum-Ultraviolet Multiphoton Spectroscopy. *J. Opt. Soc. Am. B*, vol. 10, no. 12, Dec. 1993, pp. 2273–2286.

10. Qihong, Lou; Takashi, Yagi; and Hideaki, Saito: KrF/H_2 Raman Conversion at High Repetition Rate Using a Hydrogen Gas Circulating System. *J. Appl. Phys.*, vol. 67, no. 10, May 1990, pp. 6591–6593.

11. Schomburg, H.; Döbele, H. F.; and Rückle, B.: Tunable Narrow Line Amplification in ArF* and Anti-Stokes Production Around 179 nm. *Appl. Phys. B*, vol. 28, nos. 2/3, 1982, p. 201.

12. Boyd, Gary D.; Johnston, W. Dexter, Jr.; and Kaminow, Ivan P.: Optimization of the Stimulated Raman Scattering Threshold. *IEEE J. Quant. Electron.*, vol. QE-5, no. 4, Apr. 1969, pp. 203–206.

13. Henesian, M. A.; Swift, C. D.; and Murray, J. R.: Stimulated Rotational Raman Scattering in Nitrogen in Long Air Paths. *Opt. Lett.*, vol. 10, no. 11, Nov. 1985, pp. 565–567.

14. Balla, R. Jeffrey; and Hart, R. C.: Spectral Brightness and Other Improvements to the Tunable ArF Excimer Laser. *Rev. Sci. Instrum.*, vol. 69, no. 7, July 1998, pp. 2591–2594.

15. Brueck, S. R. J.; and Kildal, Helge: Efficient Raman Frequency Conversion in Liquid Nitrogen. *IEEE J. Quant. Electron.*, vol. QE-18, no. 3, Mar. 1982, pp. 310–312.

16. Carlsten, J. L.; Telle, J. M.; and Wenzel, R. G.: Efficient Stimulated Raman Scattering Due to Absence of Second Stokes Growth. *Opt. Lett.*, vol. 9, no. 8, Aug. 1984, pp. 353–355.

17. Bragg, S. L.; Brault, J. W.; and Smith, W. H.: Line Positions and Strengths in the H_2 Quadrupole Spectrum. *Astrophys. J.*, vol. 263, Dec. 1982, pp. 999–1004.

18. Luches, A.; Nassisi, V.; and Perrone, M. R.: Stimulated Raman Scattering in H_2–Ar Mixtures. *Opt. Lett.*, vol. 12, no. 1, Jan. 1987, pp. 33–35.

19. Jennings, D. E.; and Brault, J. W.: The Ground State of Molecular Hydrogen. *J. Mol. Spectrosc.*, vol. 102, 1983, pp. 265–272.

20. Owyoung, Adelbert; Patterson, Chris W.; and McDowell, Robin S.: CW Stimulated Raman Gain Spectroscopy of the ν_1 Fundamental of Methane. *Chem. Phys. Lett.*, vol. 59, no. 1, Nov. 1978, pp. 156–162.

21. Chase, M. W., Jr.; Davies, C. A.; Downey, J. R., Jr.; Frurip, D. J.; McDonald, R. A.; and Syverud, A. N.: JANAF Thermochemical Tables—Third Edition, Part 1, Al–Co. *J. Phys. Chem. Ref. Data*, vol. 14, Suppl. 1, 1985, pp. 1–1856.

22. Murray, J. R.; Goldhar, J.; and Szöke, A.: Backward Raman Gain Measurements for KrF Laser Radiation Scattered by CH_4. *Appl. Phys. Lett.*, vol. 32, no. 9, May 1978, pp. 551–553.

23. Lancaster, D. G.; and Dawes, J. M.: A Pulsed Laser Source Using Stimulated Raman Scattering and Difference Frequency Mixing: Remote Sensing of

Methane in Air. *Opt. Comm.*, vol. 120, 1995, pp. 307–310.

24. Jones, D. C.; Mangir, M. S.; Rockwell, D. A.; and White, J. O.: Stimulated Brillouin Scattering Gain Variation and Transient Effects in a CH_4:He Binary Gas Mixture. *J. Opt. Soc. Am. B.*, vol. 7, no. 10, Oct. 1990, pp. 2090–2096.

25. Jennings, Donald E.; Weber, A.; and Brault, J. W.: Raman Spectroscopy of Gases With a Fourier Transform Spectrometer: The Spectrum of D_2. *Appl. Opt.*, vol. 25, no. 2, Jan. 1986, pp. 284–290.

26. Lofthus, Alf; and Krupenie, Paul H.: The Spectrum of Molecular Nitrogen. *J. Phys. Chem. Ref. Data*, vol. 6, no. 1, 1977, pp. 113–307.

27. Lempert, W. R.; Zhang, B.; Miles, R. B.; and Looney, J. P.: Stimulated Raman Scattering and Coherent Anti-Stokes Raman Spectroscopy in High-Pressure Oxygen. *J. Opt. Soc. Am. B.*, vol. 7, no. 5, May 1990, pp. 715–721.

28. Esherick, Peter; and Owyoung, Adelbert: High-Resolution Stimulated Raman Gain Spectrum of the ν_1 Band of SF_6. *J. Mol. Spectrosc.*, vol. 92, 1982, pp. 162–169.

29. Esherick, Peter; and Owyoung, Adelbert: High Resolution Stimulated Raman Spectroscopy. *Advances in Infrared and Raman Spectroscopy—Volume 9*, R. J. H. Clark and R. E. Hester, eds., Heyden & Sons, Ltd., 1982, pp. 130–187.

30. Tomov, I. V.; Fedosejevs, R.; and McKen, D. C. D.: High-Efficiency Stimulated Brillouin Scattering of KrF Laser Radiation in SF_6. *Opt. Lett.*, vol. 9, no. 9, Sept. 1984, pp. 405–407.

31. Mack, M. E.; Carman, R. L.; Reintjes, J.; and Bloembergen, N.: Transient Stimulated Rotational and Vibrational Raman Scattering in Gases. *Appl. Phys. Lett.*, vol. 16, no. 5, Mar. 1970, pp. 209–211.

32. Frey, R.; Lukasik, J.; and Ducuing, J.: Tunable Raman Excitation and Vibrational Relaxation in Diatomic Molecules. *Chem. Phys. Lett.*, vol. 14, no. 4, June 1972, pp. 514–517.

33. Millikan, Roger C.; and White, Donald R.: Systematics of Vibrational Relaxation. *J. Chem. Phys.*, vol. 39, no. 12, Dec. 1963, pp. 3209–3213.

34. Akhmanov, S. A.; Khokhlov, R. V.; and Sukhorukov, A. P.: Self-Focusing, Self-Defocusing and Self-Modulation of Laser Beams. *Laser Handbook*, Volume 2, F. T. Arecchi and E. O. Schulz-Dubois, eds., North-Holland Publ. Co., 1972, pp. 1151–1228.

35. Smith, David C.: High-Power Laser Propagation: Thermal Blooming. *Proc. IEEE*, vol. 65, no. 12, Dec. 1977, pp. 1679–1714.

36. DeMartini, F.; and Ducuing, J.: Stimulated Raman Scattering in Hydrogen: A Measurement of the Vibrational Lifetime. *Phys. Rev. Lett.*, vol. 17, no. 3, July 1966, pp. 117–119.

37. Audibert, M.-M.; Joffrin, C.; and Ducuing, J.: Vibrational Relaxation of H_2 in the Range 500–40°K. *Chem. Phys. Lett.*, vol. 25, no. 2, Mar. 1974, pp. 158–163.

38. Audibert, M.-M.; Joffrin, C.; and Ducuing, J.: Vibrational Relaxation in Hydrogen—Rare-Gases Mixtures. *Chem. Phys. Lett.*, vol. 19, no. 1, Mar. 1973, pp. 26–28.

39. Hess, Peter; and Moore, C. Bradley: Vibrational Energy Transfer in Methane and Methane-Rare-Gas Mixtures. *J. Chem. Phys.*, vol. 65, no. 6, Sept. 1976, pp. 2339–2344.

40. Lukasik, J.; and Ducuing, J.: Vibrational Relaxation of D_2 in the Range 400–50°K. *Chem. Phys. Lett.*, vol. 27, no. 2, July 1974, pp. 203–205.

41. Lukasik, Jacques: Vibrational Relaxation of D_2 in Collisions With He in the Range 400–80 K. *Chem. Phys. Lett.*, vol. 44, no. 2, Dec. 1976, pp. 219–220.

42. Gladkov, S. M.; Karimov, M. G.; and Koroteev, N. I.: Two-Photon Raman Excitation and Coherent Anti-Stokes Raman Spectroscopy Probing of Population Changes in Polyatomic Molecules: A Novel Nonlinear Optical Technique for Vibrational-Relaxation Studies. *Opt. Lett.*, vol. 8, no. 6, June 1983, pp. 298–300.

43. Gebhardt, Frederick G.; and Smith, David C.: Effects of Wind on Thermal Defocusing of CO_2 Laser Radiation. *Appl. Phys. Lett.*, vol. 14, no. 2, Jan. 1969, pp. 52–54.

44. Touloukian, Y. S.; Liley, P. E.; and Saxena, S. C.: *Thermal Conductivity—NonMetallic Liquids and Gases, Thermophysical Properties of Matter: Volume 3*. IFI/Plenum, 1970.

45. Ahlberg, Kersti, ed.: *AGA Gas Handbook*. Almqvist & Wiksell Internat., 1985, p. 81.

46. Zhang, Boying Barry: Stimulated Raman Scattering in High Pressure Oxygen and Its Role in the Relief (Raman Excitation + Laser Induced Fluorescence) Flow Tagging Technique. Ph.D Diss., Princeton Univ., June 1994.

47. Hirschfelder, Joseph O.; Curtiss, Charles F.; and Bird, R. Byron: *Molecular Theory of Gases and Liquids*. John Wiley & Sons, Inc., 1954.

Table 1. Vibrational Branch Stokes Energy Conversion in CF_4

[Data acquired using 40 mJ of pump laser energy and a 5-Hz repetition rate]

Density, amagats		Energy generated, μJ				
CF_4	He	Q_1	Q_2	Q_3	Q_4	Q_{-1}
4.1	0	0	0	0	0	0
16.6	0	7	0	0	0	0
18.5	0	14	0	0	0	0
18.5	6.3	142	6	≈1	≈1	≈1
18.5	12.6	140	5	≈1	≈1	≈1

Table 2. Accessible Frequency Ranges and Maximum Energy Conversions Obtainable by SRS Using a FCRC and Tunable ArF Excimer

[Conversions are obtained at laser frequency of 51 714 cm^{-1} and conditions that optimize conversion for each particular transition]

Gas	Transition	Frequency range, cm^{-1}	Energy conversion, percent
H_2	$Q_{0,-1}$	52 460–52 160	0.35
D_2	$Q_{0,-1}$	52 285–51 985	0.75
D_2	$Q_{0,+1}$	51 455–51 155	2.5
H_2	$Q_{0,+1}$	51 280–50 980	1.3
SF_6	Q_1	51 095–50 795	2.1
D_2	$Q_{0,+2}$	51 040–50 740	0.002
CF_4	Q_1	50 960–50 660	0.35
H_2	$Q_{0,+2}$	50 695–50 395	0.053
SF_6	Q_2	50 320–50 020	0.26
H_2	$Q_{0,+3}$	50 110–49 810	0.0033
CF_4	Q_2	50 050–49 750	0.015
D_2	$Q_{1,-2}$	49 710–49 410	0.006
N_2	Q_1	49 540–49 240	21
H_2	$Q_{0,+4}$	49 520–49 220	0.00012
D_2	$Q_{1,-1}$	49 295–48 995	0.6
CH_4	Q_1	48 955–48 655	22
H_2	$Q_{1,-2}$	48 890–48 590	0.012
D_2	Q_1	48 880–48 580	53
D_2	$Q_{1,+1}$	48 470–48 170	2
H_2	$Q_{1,-1}$	48 300–48 000	1.2
D_2	$Q_{1,+2}$	48 055–47 765	0.02
H_2	Q_1	47 715–47 415	20
H_2	$Q_{1,+1}$	47 130–46 830	3
D_2	$Q_{2,-2}$	46 725–46 425	0.002
H_2	$Q_{1,+2}$	46 540–46 240	0.033
D_2	$Q_{2,-1}$	46 310–46 010	0.45
CH_4	Q_2	46 040–45 740	28
H_2	$Q_{1,+3}$	45 955–45 655	0.0045
D_2	Q_2	45 895–45 595	23
D_2	$Q_{2,+1}$	45 480–45 180	1.6
D_2	$Q_{2,+2}$	45 065–44 765	0.008
H_2	$Q_{2,-2}$	44 735–44 435	0.0055
H_2	$Q_{2,-1}$	44 145–43 845	0.9
H_2	Q_2	43 560–43 260	35
D_2	$Q_{3,-1}$	43 325–43 025	0.2
CH_4	Q_3	43 120–42 820	0.032
H_2	$Q_{2,+1}$	42 975–42 675	3.1
D_2	Q_3	42 910–42 610	13
D_2	$Q_{3,+1}$	42 495–42 195	0.9
H_2	$Q_{2,+2}$	42 385–42 085	0.062
H_2	$Q_{3,-1}$	39 990–39 690	0.45
D_2	Q_4	39 920–39 620	2.6
H_2	Q_3	39 405–39 105	11
H_2	$Q_{3,+1}$	38 820–38 520	0.98
H_2	$Q_{4,-1}$	35 835–35 535	0.042
H_2	Q_4	35 250–34 950	4
H_2	$Q_{4,+1}$	34 660–34 360	0.055

Table 3. Vibrational Relaxation Data for $v = 1$

Molecule pair		$p\tau$, atm-s	Reference	Temperature, K
H_2	H_2	$1060 \pm 100 \times 10^{-6}$	36	300
		385×10^{-6}	37	295
	He	2280×10^{-6}	38	298
CH_4	CH_4	$5.1 \pm 0.8 \times 10^{-9}$	39	295
	He	$1.7 \pm 0.3 \times 10^{-8}$	39	295
D_2	D_2	$2.87 \pm 0.19 \times 10^{-3}$	40	296
	He	6×10^{-3}	41	296
N_2	N_2	$3.2 \times 10^{+3}$	[a]33	300
		>1	32	298
	He	$6.9 \pm 0.3 \times 10^{-3}$	32	298
		1.5×10^{-2}	[a]33	298
SF_6	SF_6	$>2 \times 10^{-8}$	42	300
CF_4	CF_4	No data available		

[a]Extrapolated to ≈300 K from high temperature measurements.

Table 4. 10-Hz Thermal Diffusion Lengths $L(10)$

Gas	C_p, J/mol-K	k, J/m-s-K	ρ, amagats	$L(10)$, μm
He	20.8	0.15	20	2500
H_2	28.8	0.182	20	2400
D_2	29.2	0.14	26	1800
CH_4	35.6	0.034	7	1600
N_2	29.1	0.026	40	600
CF_4	61	0.016	18.5	500
SF_6	97	0.015	18	400

Table 5. Half-Stokes-Power Thermal Diffusion Lengths $L(f_{1/2})$

[For O_2-He, D = 300 μm; for all others, D = 167 μm]

Gas	Stokes order	$f_{1/2}$, Hz	ρ, amagats	$L(f_{1/2})$, μm	$L(f_{1/2})$/D
H_2	3	79	20	2400	5.1
D_2	2	64	26	1800	4.3
CH_4	1	42	7	1600	4.6
O_2-He (8:9)	1 (back)	≈3	65	1484	4.9
O_2-He (2:3)	1 (forward)	≈8	63	923	3.1

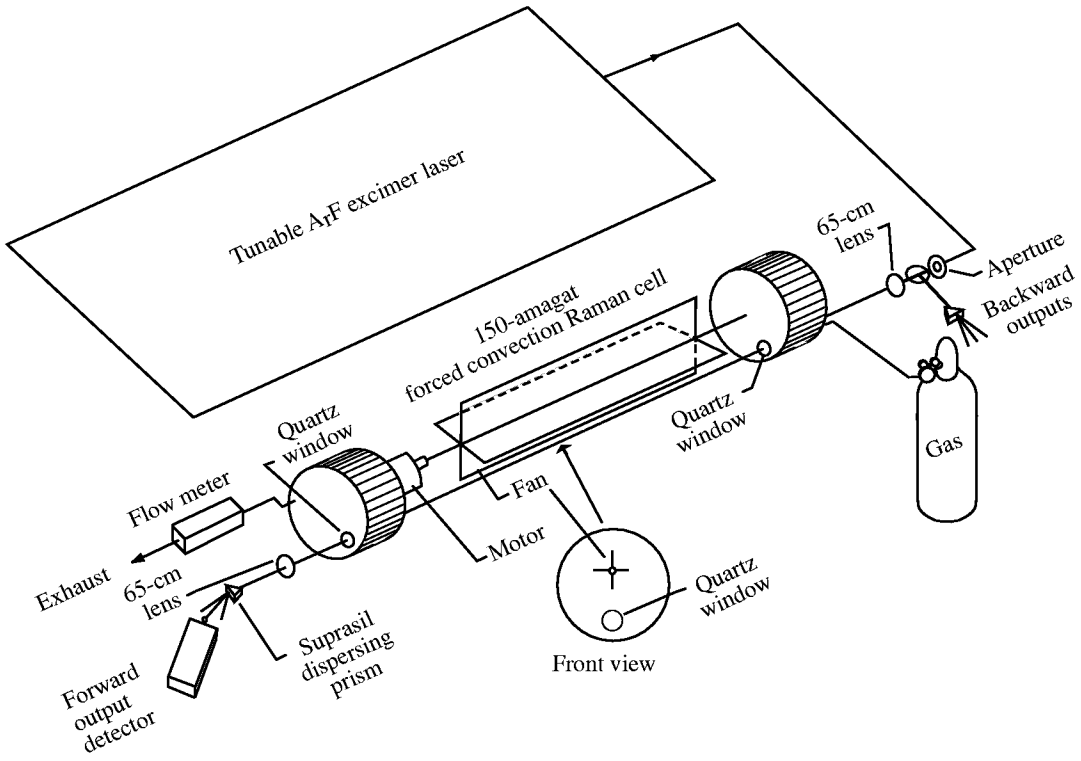

Figure 1. Schematic diagram of apparatus for Raman shifting using tunable ArF laser and forced convection Raman cell.

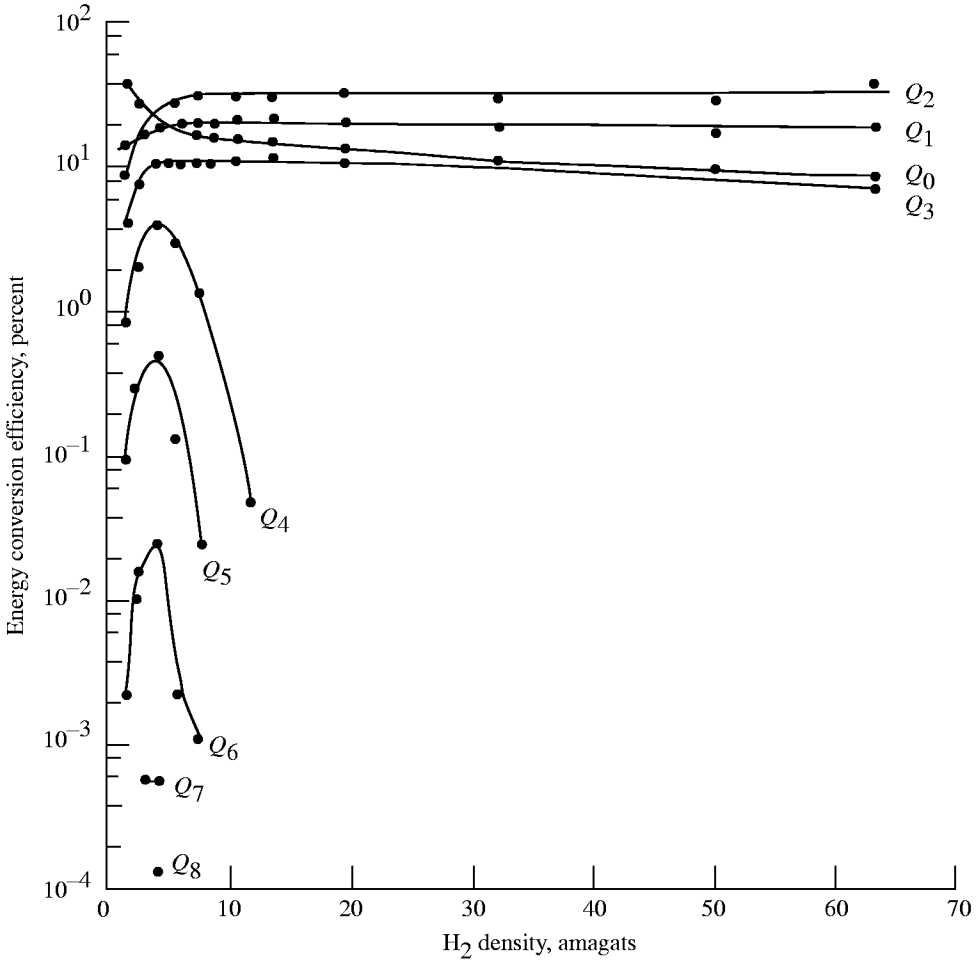

Figure 2. Conversion in H_2 at pump energy (E_{pump}) of 83 mJ versus density.

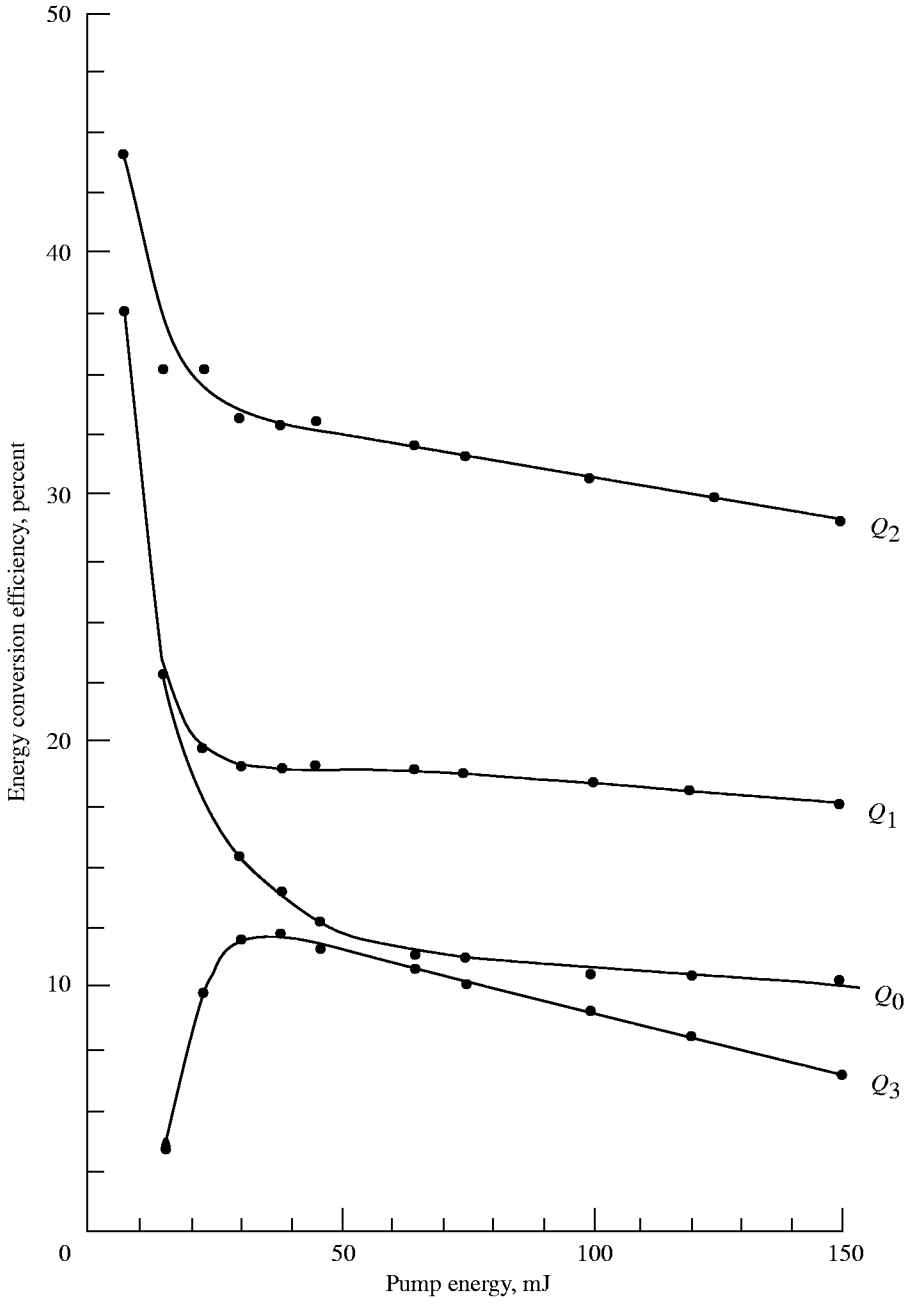

Figure 3. Conversion using 20-amagat H_2 versus input pump energy.

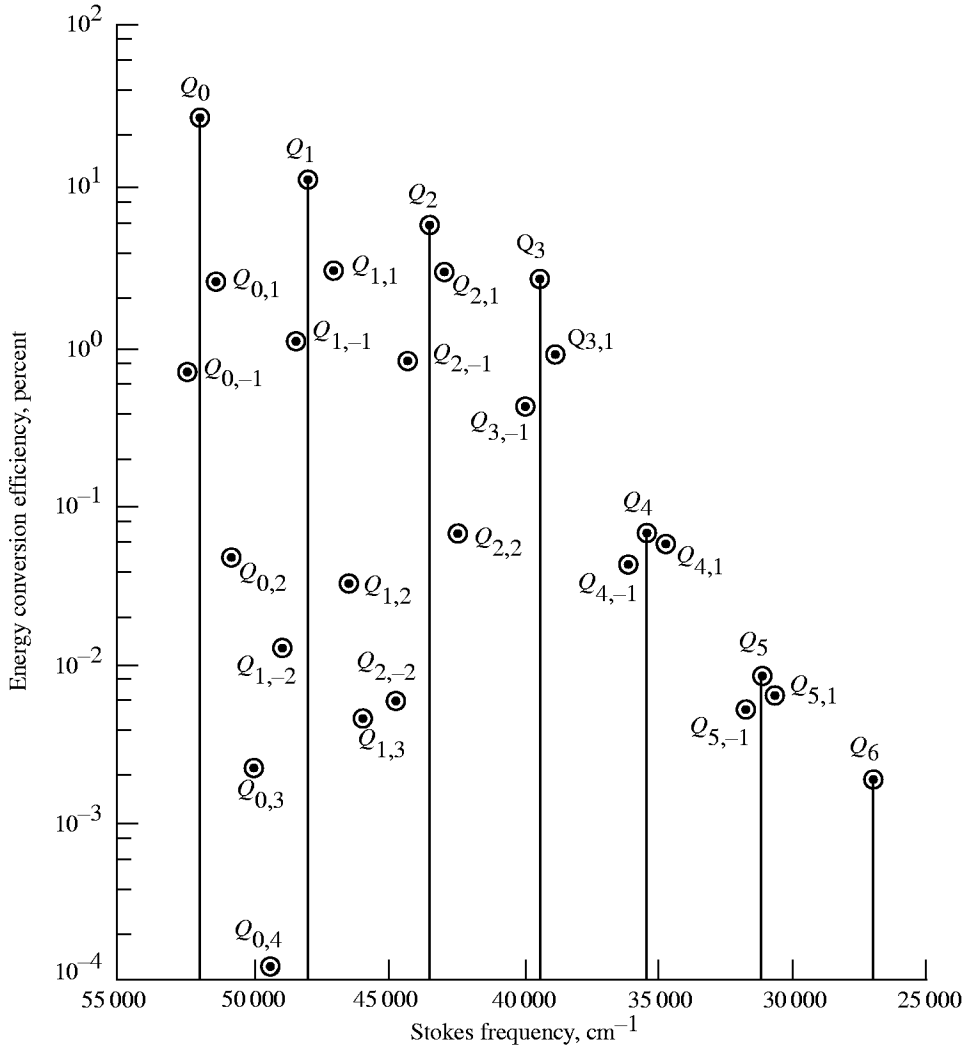

Figure 4. Summary of SRS transitions and conversions observed in 1.55-amagat H_2 with pump energy of 101 mJ.

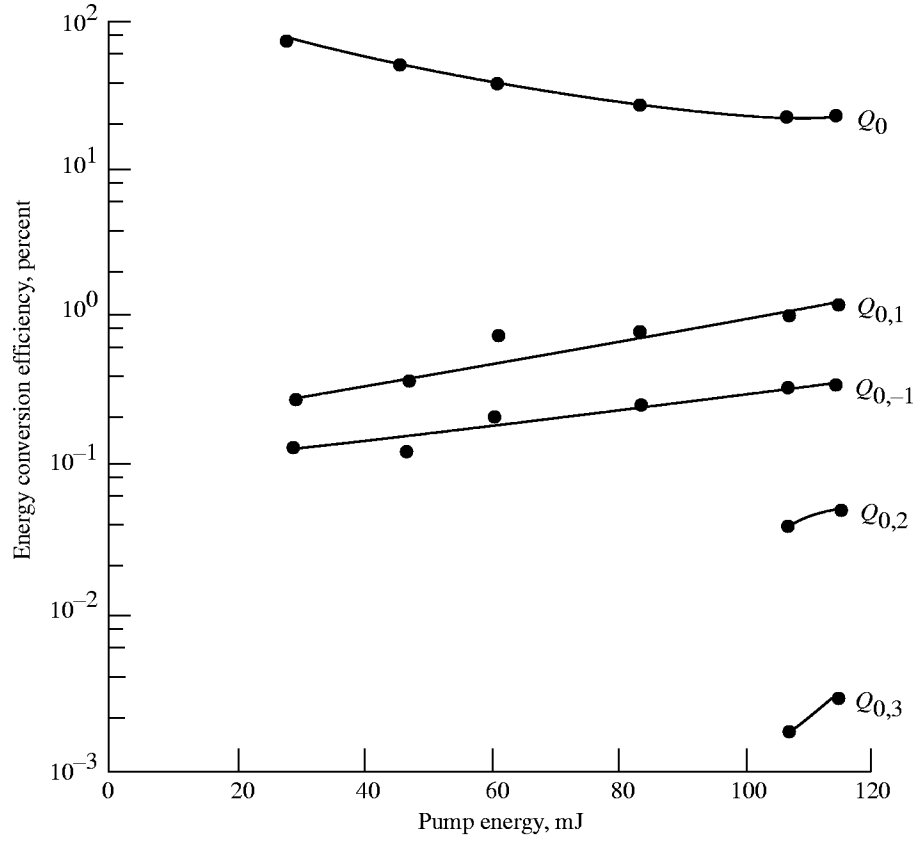

(a) Q_0.

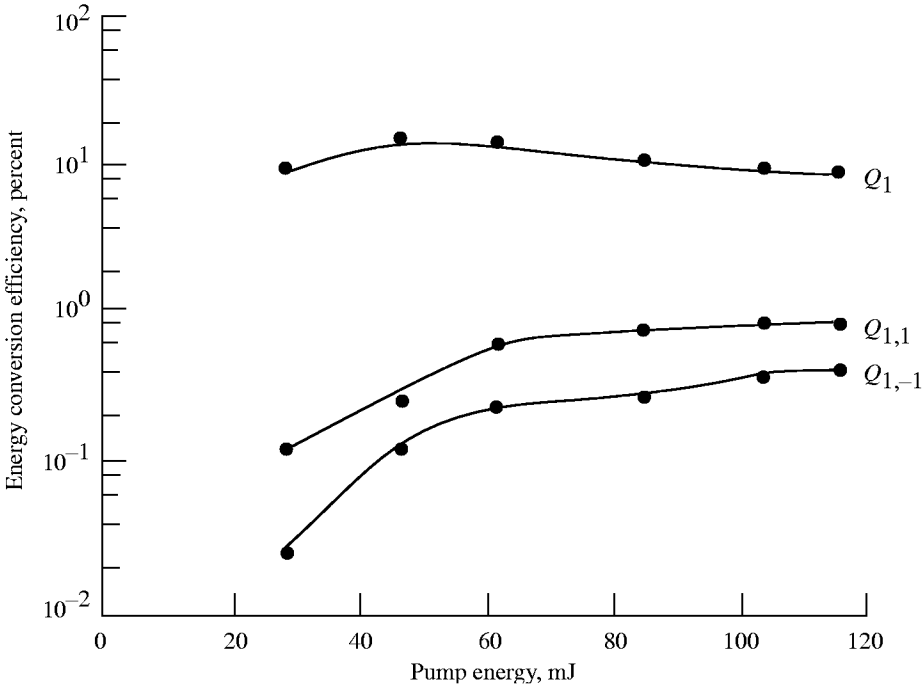

(b) Q_1.

Figure 5. SRS pure rotational transitions and conversions observed in 1.55-amagat H_2 versus pump energy.

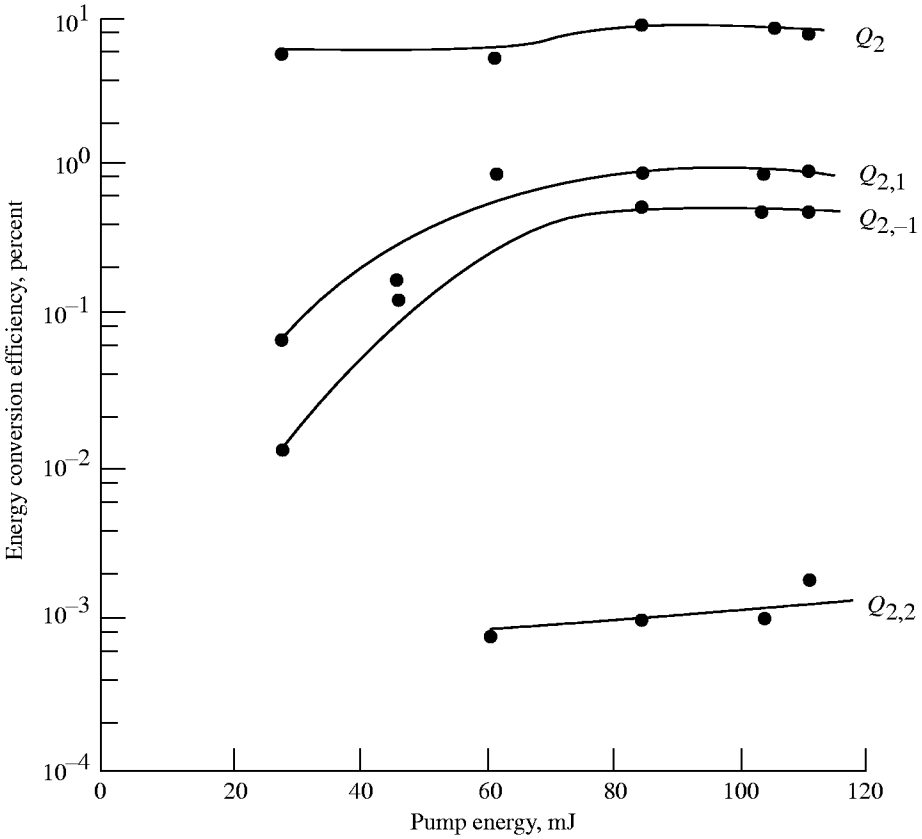

(c) Q_2.

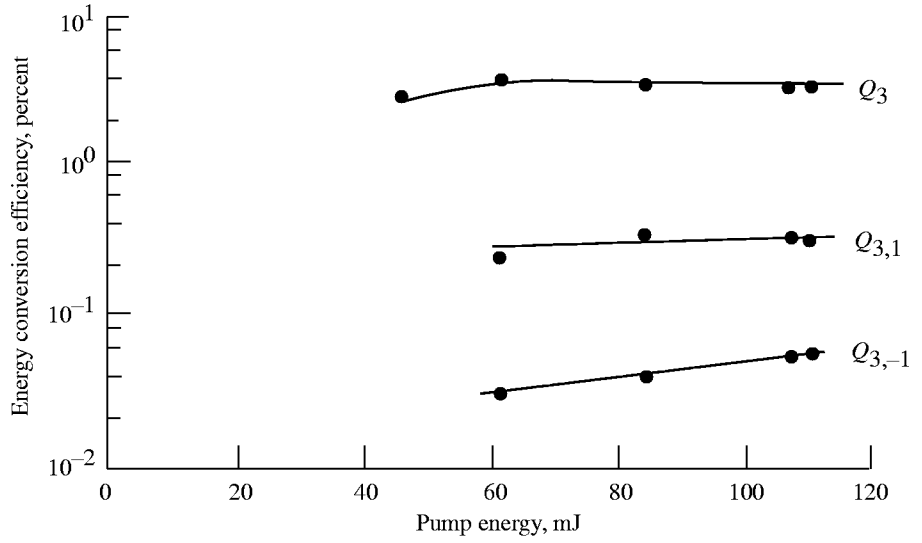

(d) Q_3.

Figure 5. Concluded.

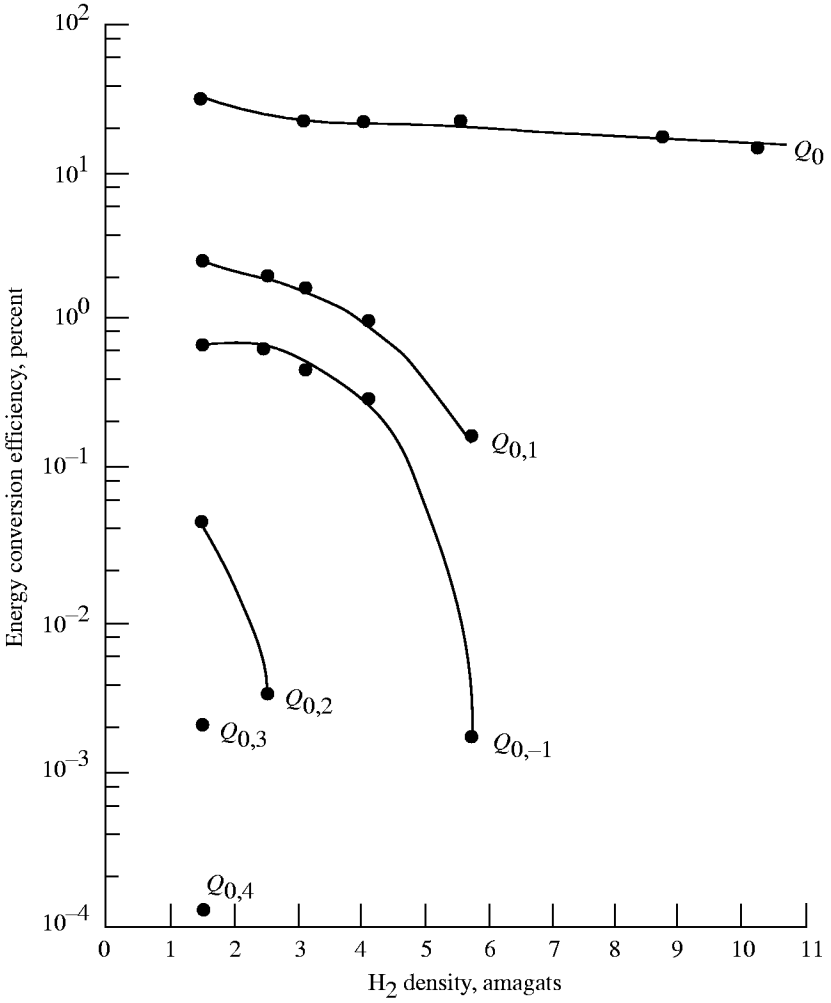

(a) Q_0.

Figure 6. SRS pure rotational transitions and conversions observed versus H_2 density using pump laser energy of 107 mJ.

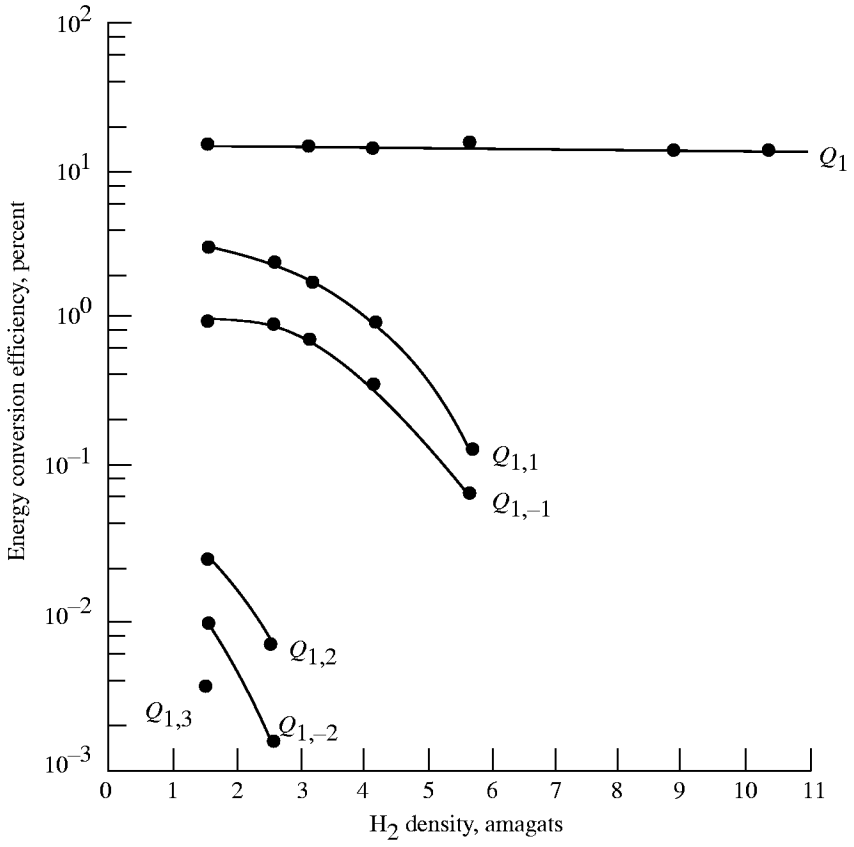

(b) Q_1.

Figure 6. Continued

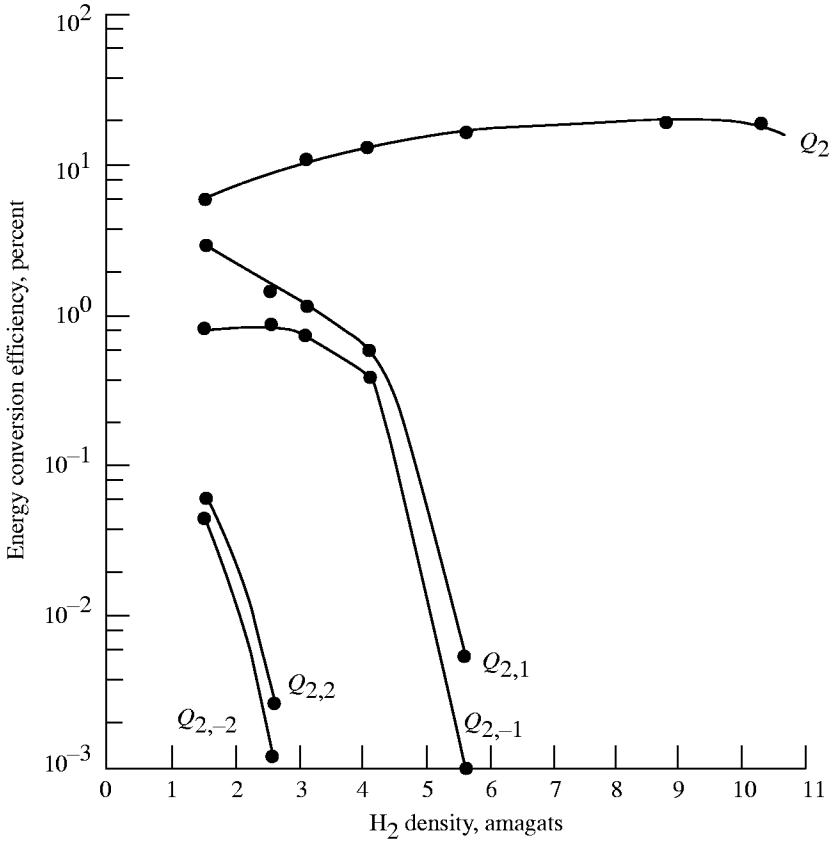

(c) Q_2.

Figure 6. Continued.

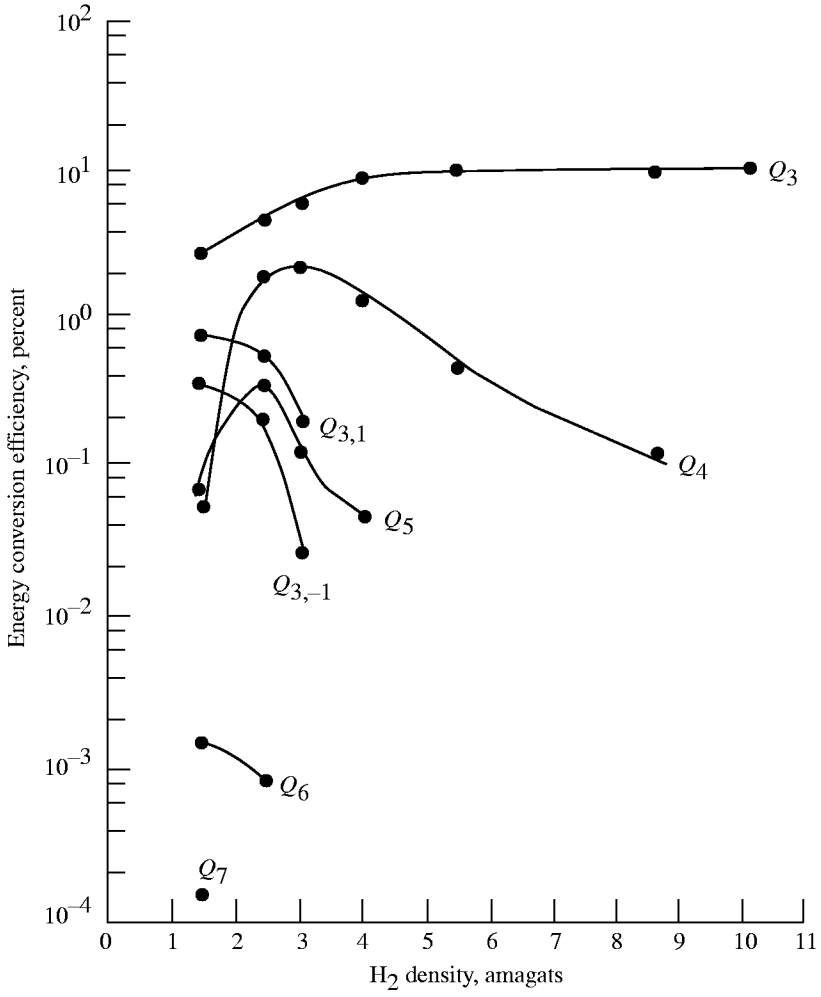

(d) Q_3.

Figure 6. Concluded.

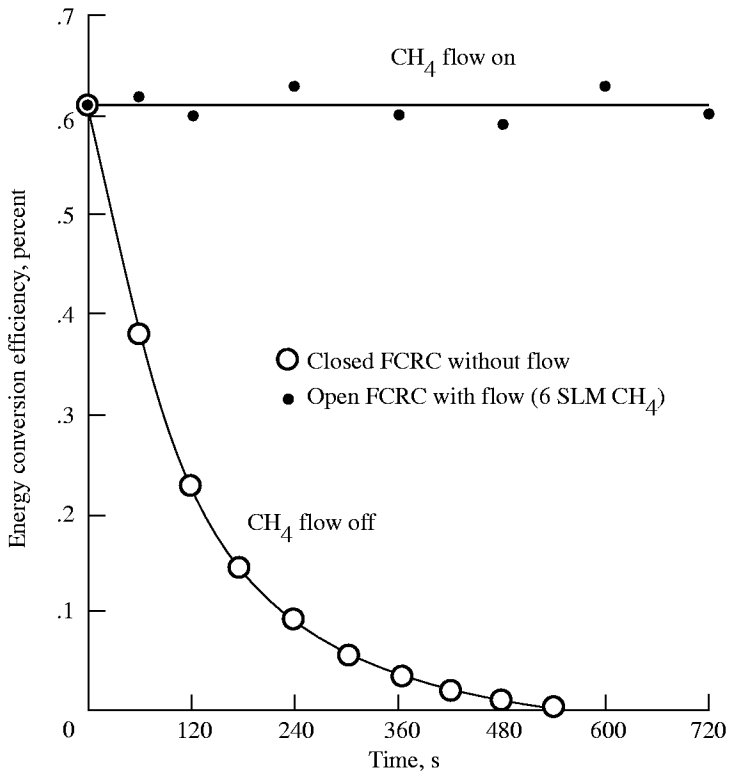

Figure 7. Conversion in 2.5-amagat CH_4 versus time at pump of energy 45 mJ and repetition rate of 5 Hz. The FCRC fan is on for both data sets.

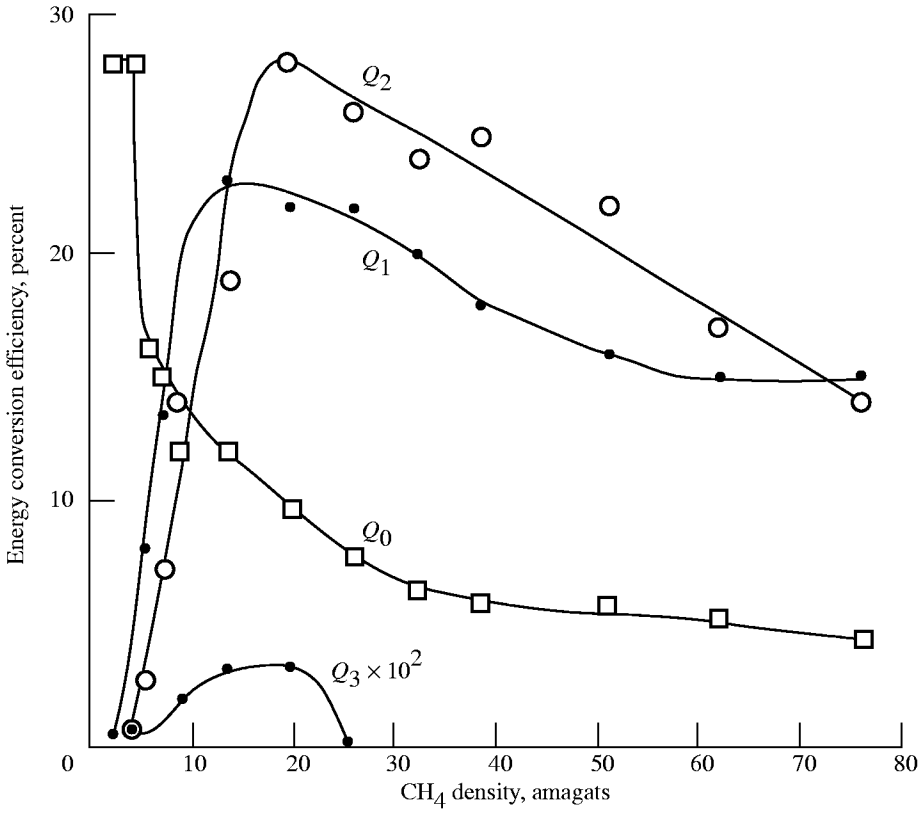

Figure 8. Conversion versus CH_4 density using pump energy of 45 mJ.

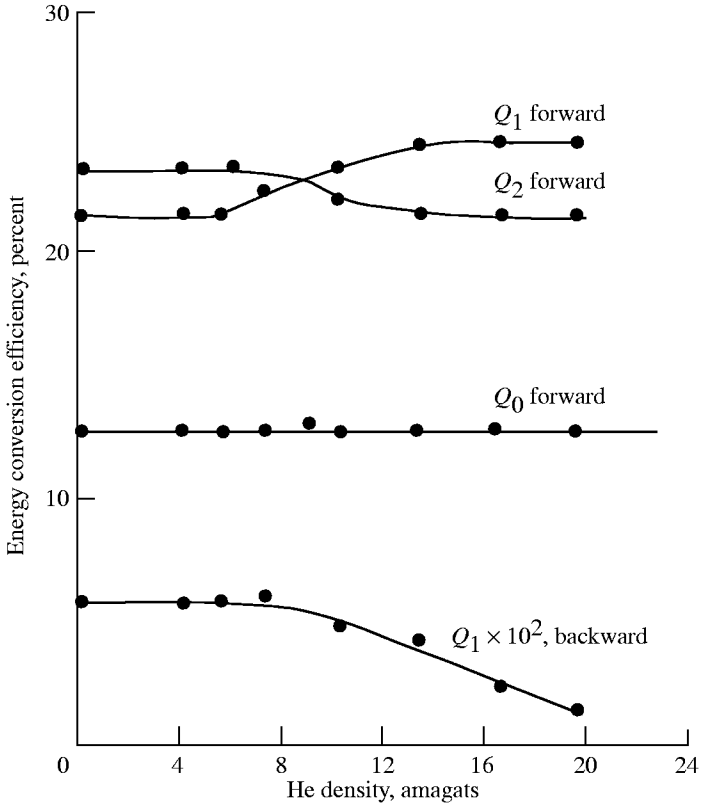

Figure 9. Forward and backward Stokes conversion in 19.7-amagat CH_4 versus helium partial density using pump energy of 42 mJ.

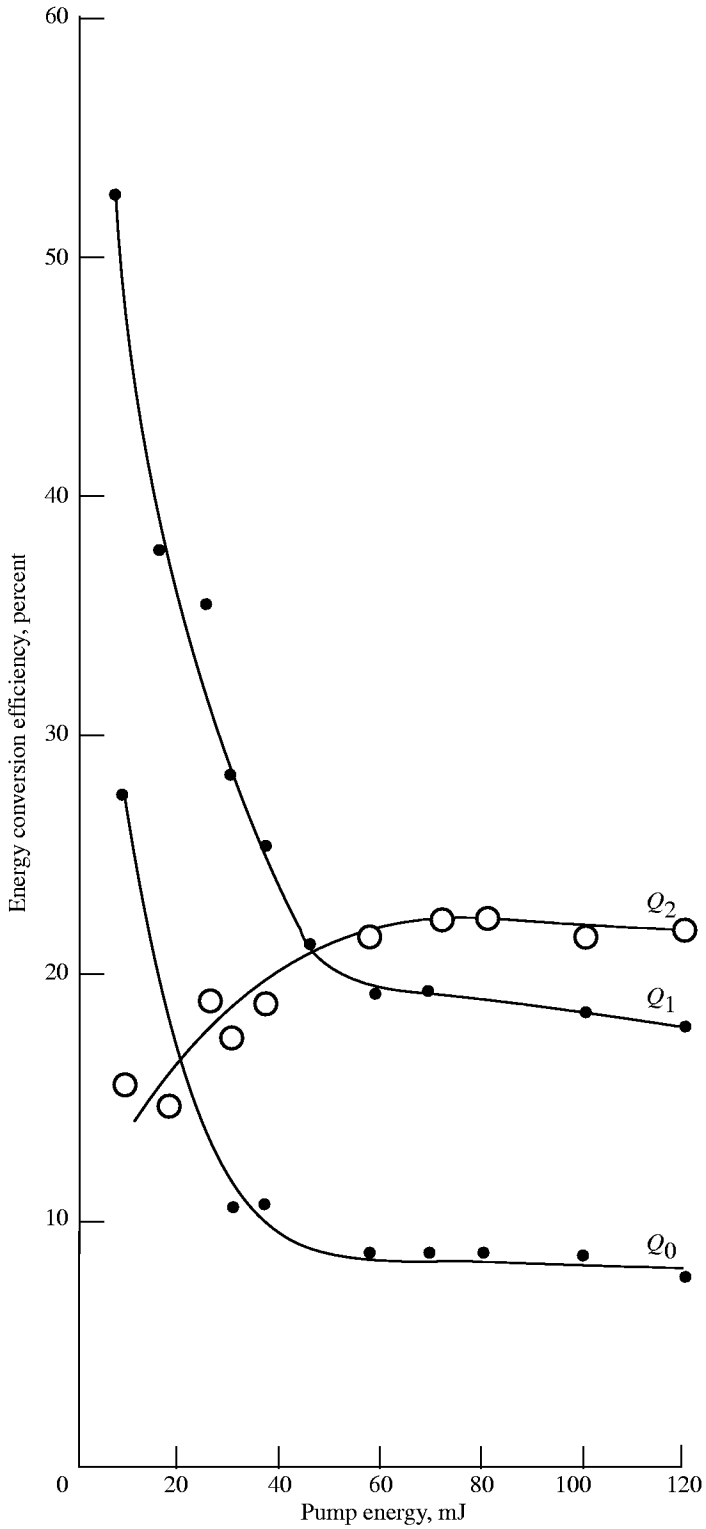

Figure 10. Conversion in 19.7-amagat pure CH_4 versus pump energy.

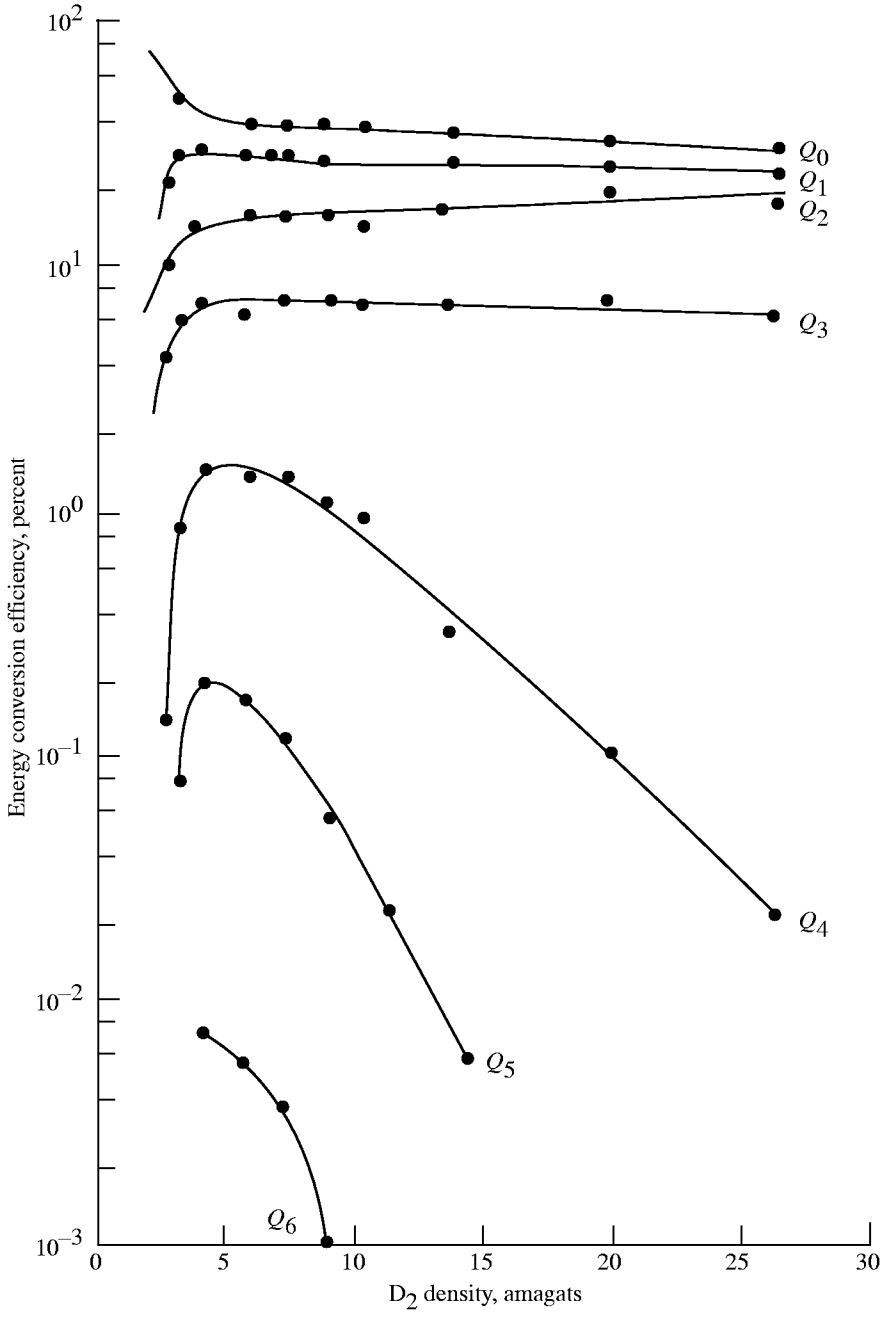

Figure 11. Conversion in D_2 versus density for pump energy of 53 mJ.

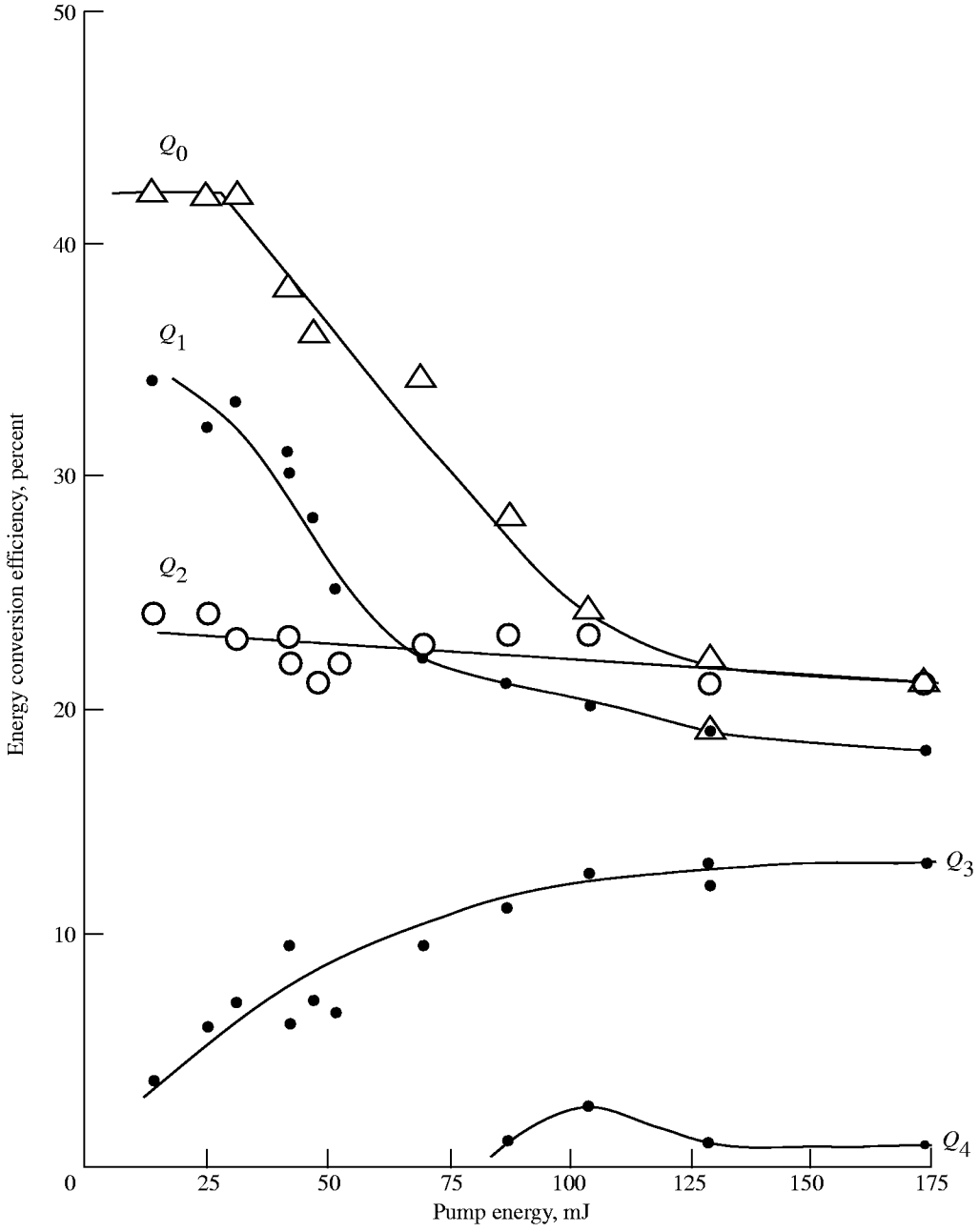

Figure 12. Conversion in 26-amagat D_2 versus pump energy.

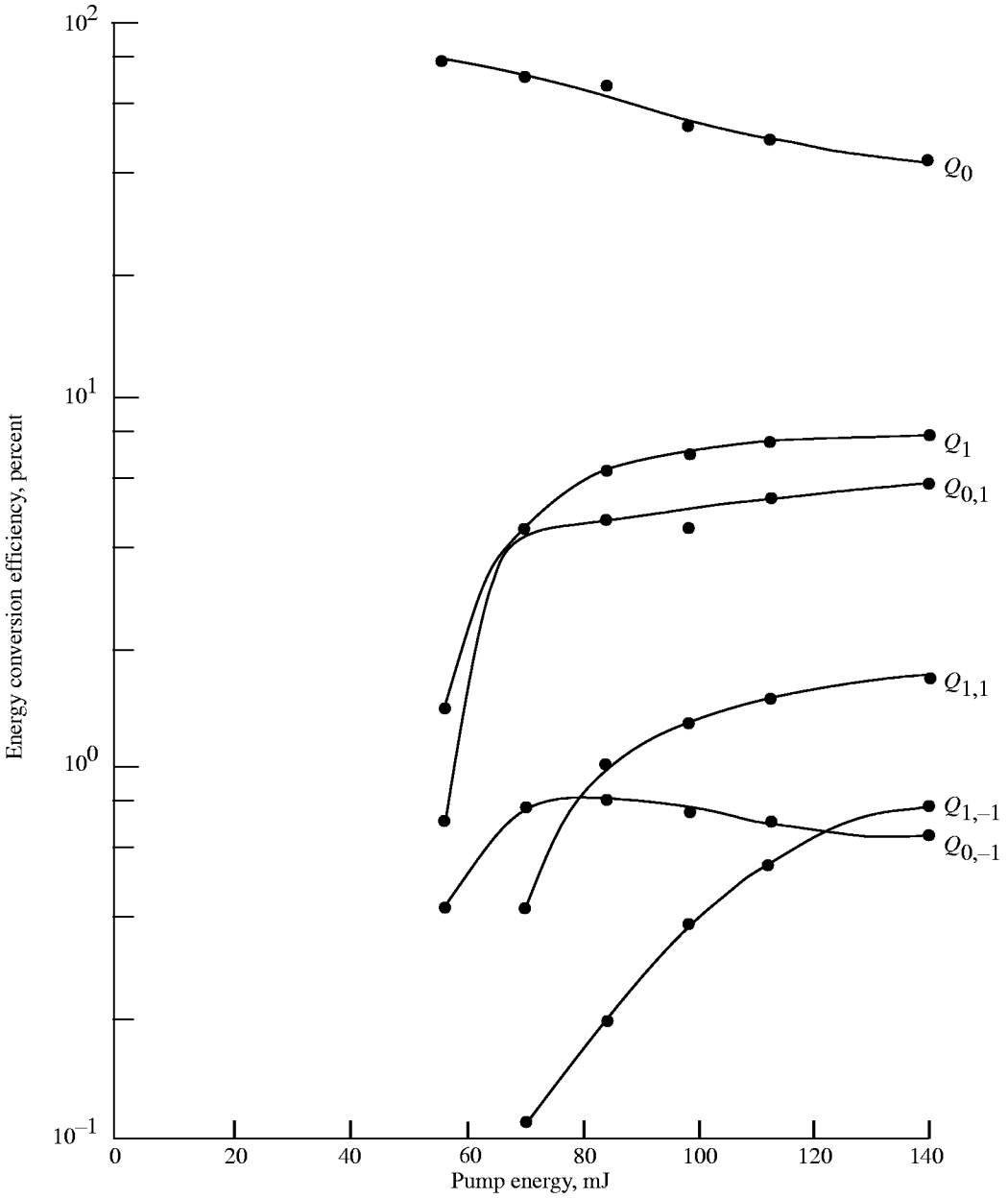

Figure 13. Conversions of transitions observed in 1.55-amagat D_2 versus pump energy.

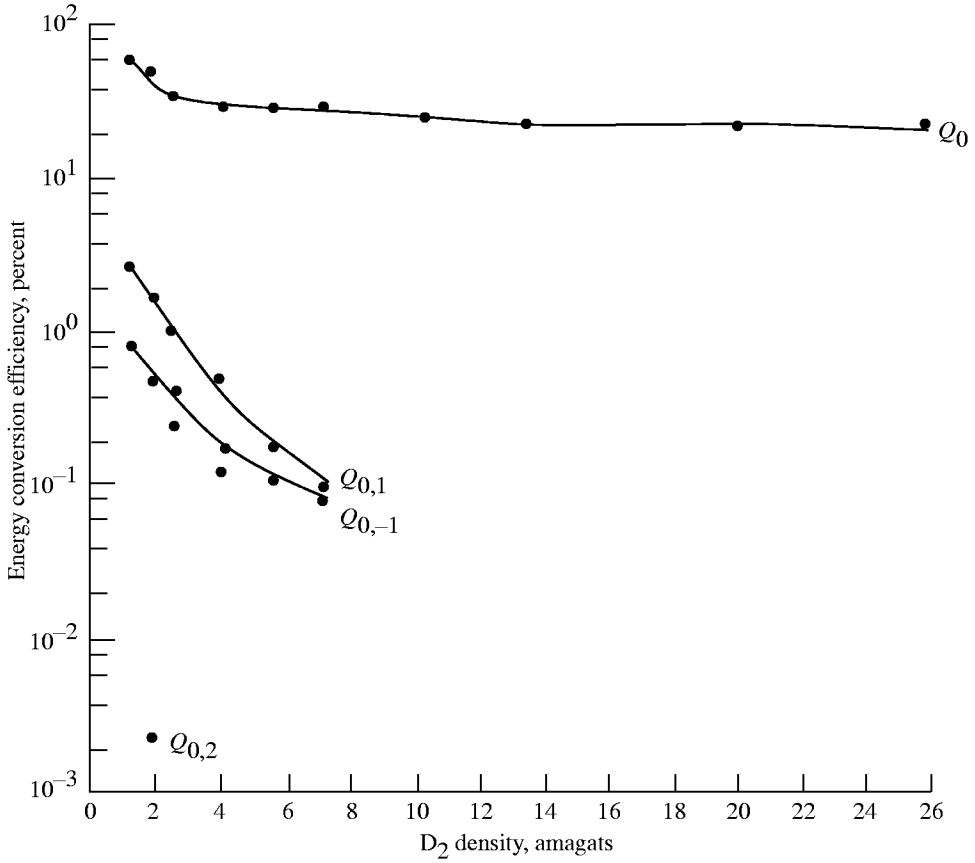

(a) Q_0.

Figure 14. Conversions of transitions observed in D_2 versus density using pump energy of 110 mJ.

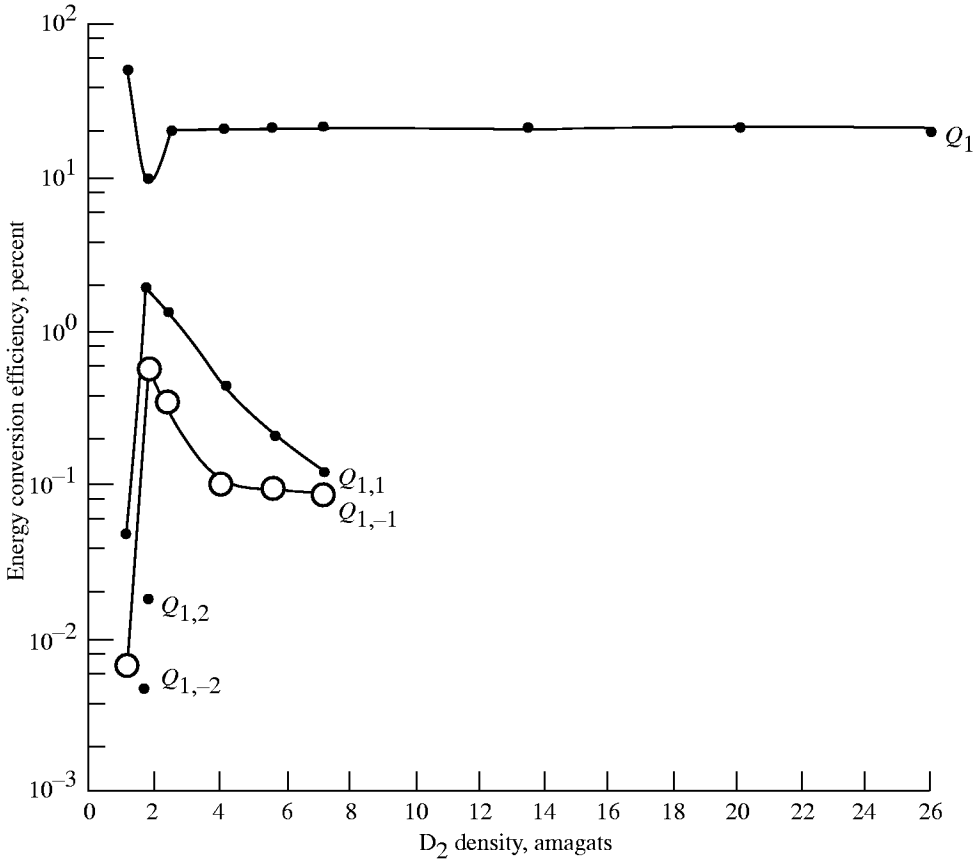

(b) Q_1.

Figure 14. Continued.

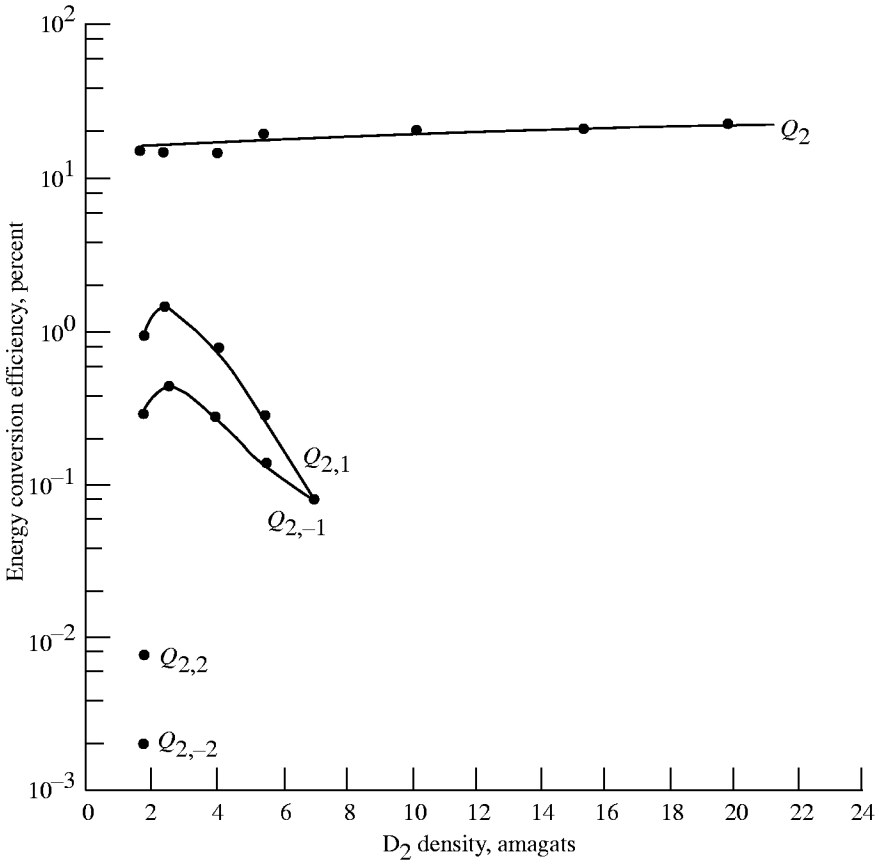

(c) Q_2.

Figure 14. Continued.

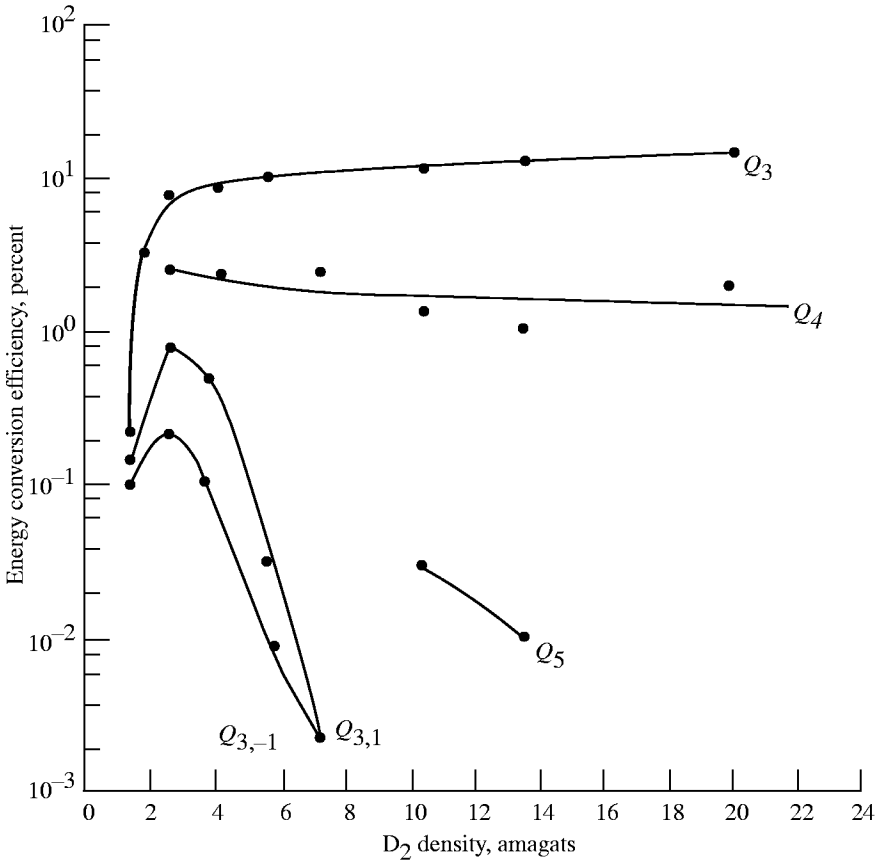

(d) Q_3, Q_4, and Q_5.

Figure 14. Concluded.

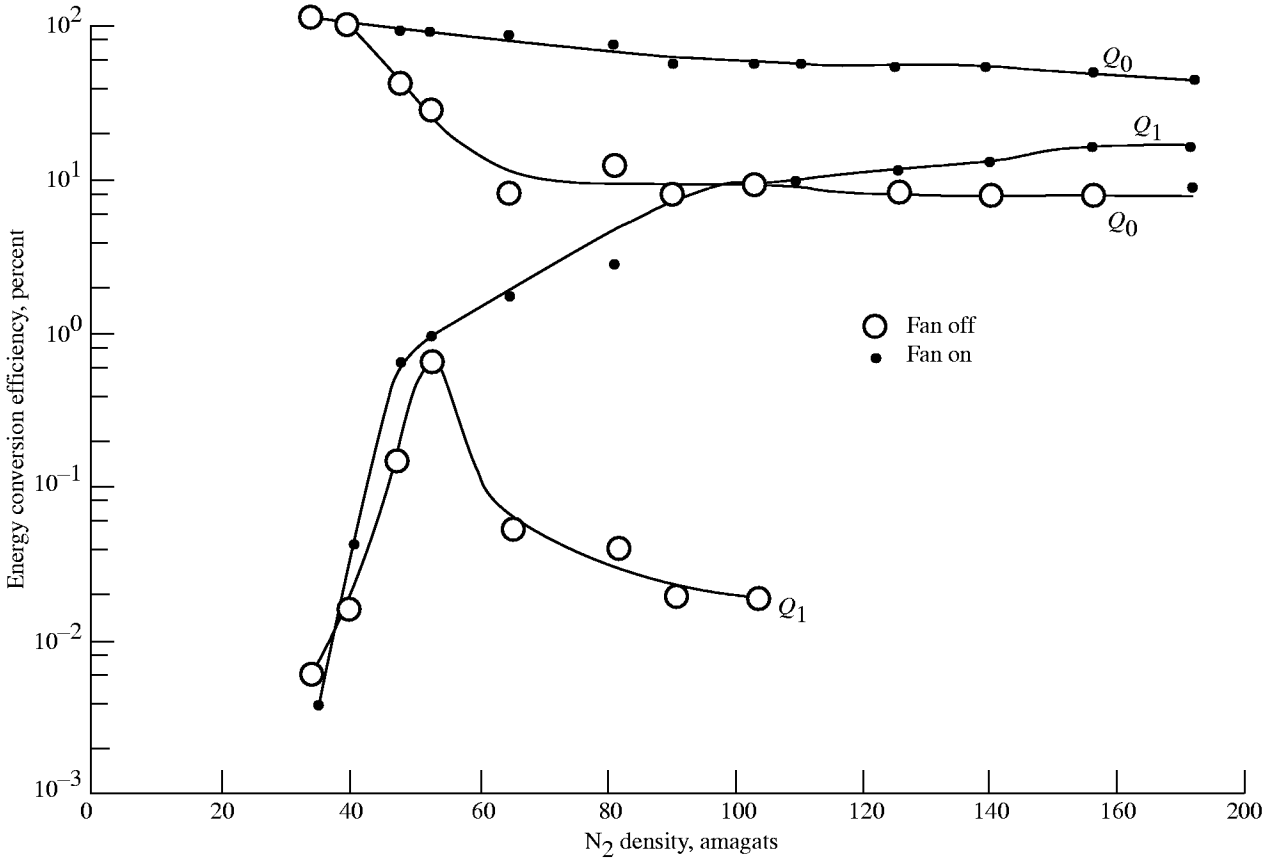

Figure 15. Conversion in pure N_2 versus density using pump energy of 45 mJ at 5 Hz.

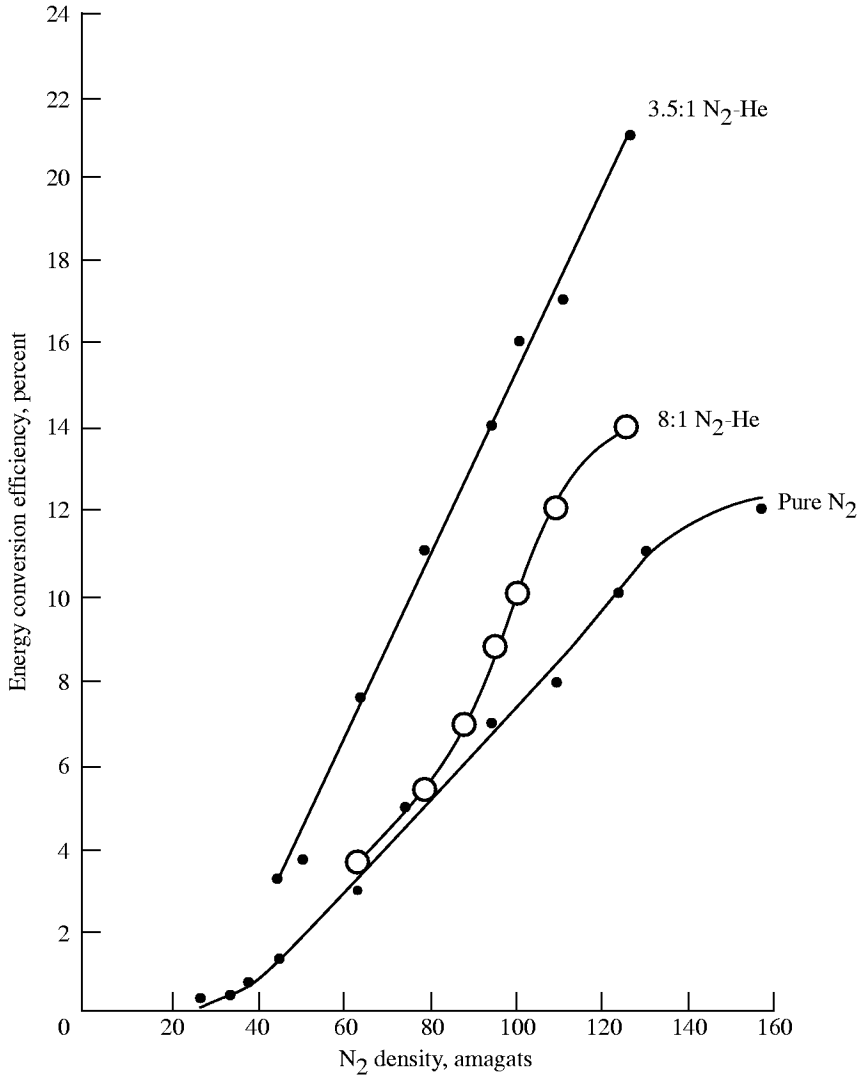

Figure 16. Forward conversion Q_1 in pure N_2 and N_2-He mixtures versus N_2 and using pump energy of 53 mJ at 5 Hz.

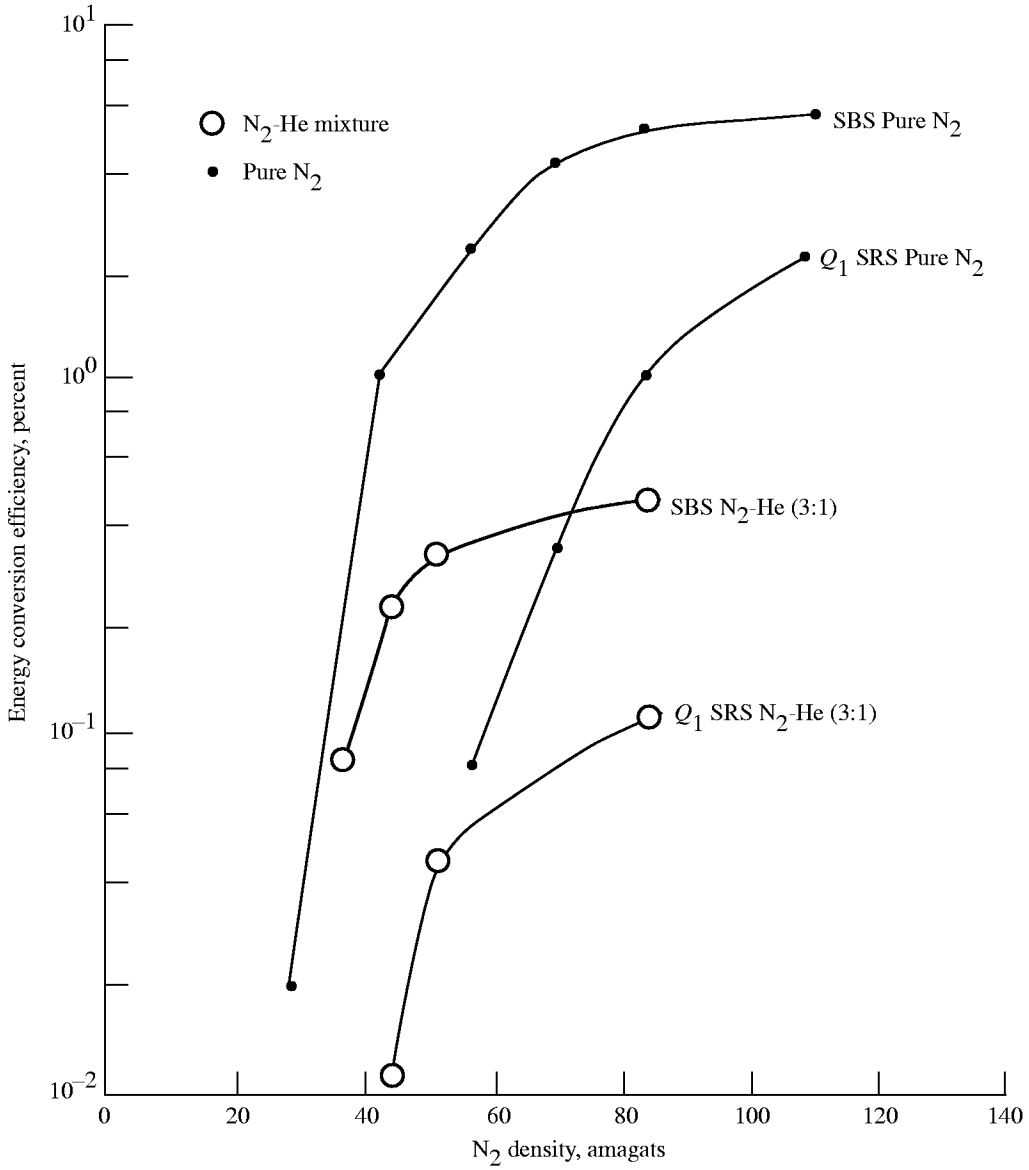

Figure 17. Backward SRS Stokes Q_1 and backward SBS conversion efficiencies in pure N_2 and a 3:1 N_2-He mixture for pump laser energy of 82 mJ at 5 Hz.

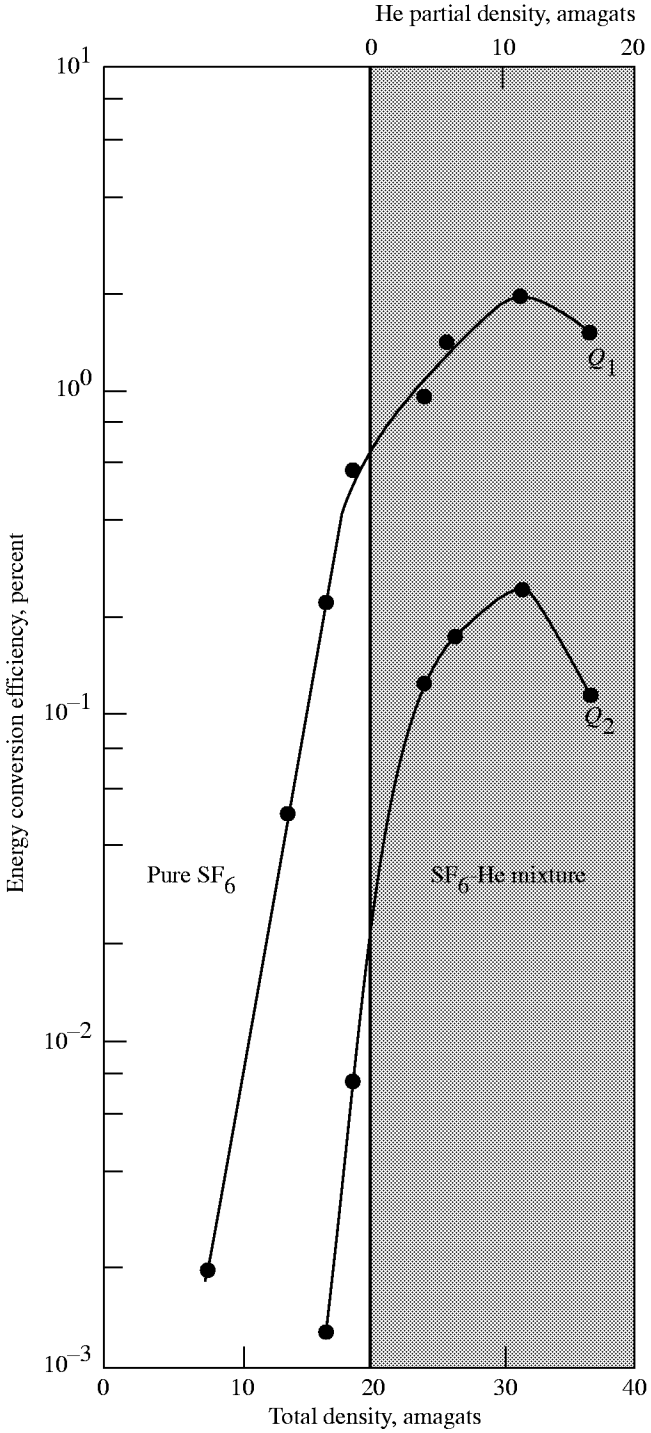

Figure 18. Conversion in SF_6 versus SF_6 density and He density using input pump energy of 59 mJ at 3 Hz with fan on. Unshaded part of figure shows conversion in pure SF_6 versus density and shaded part shows conversion versus partial He density at fixed SF_6 density of 20 amagats.

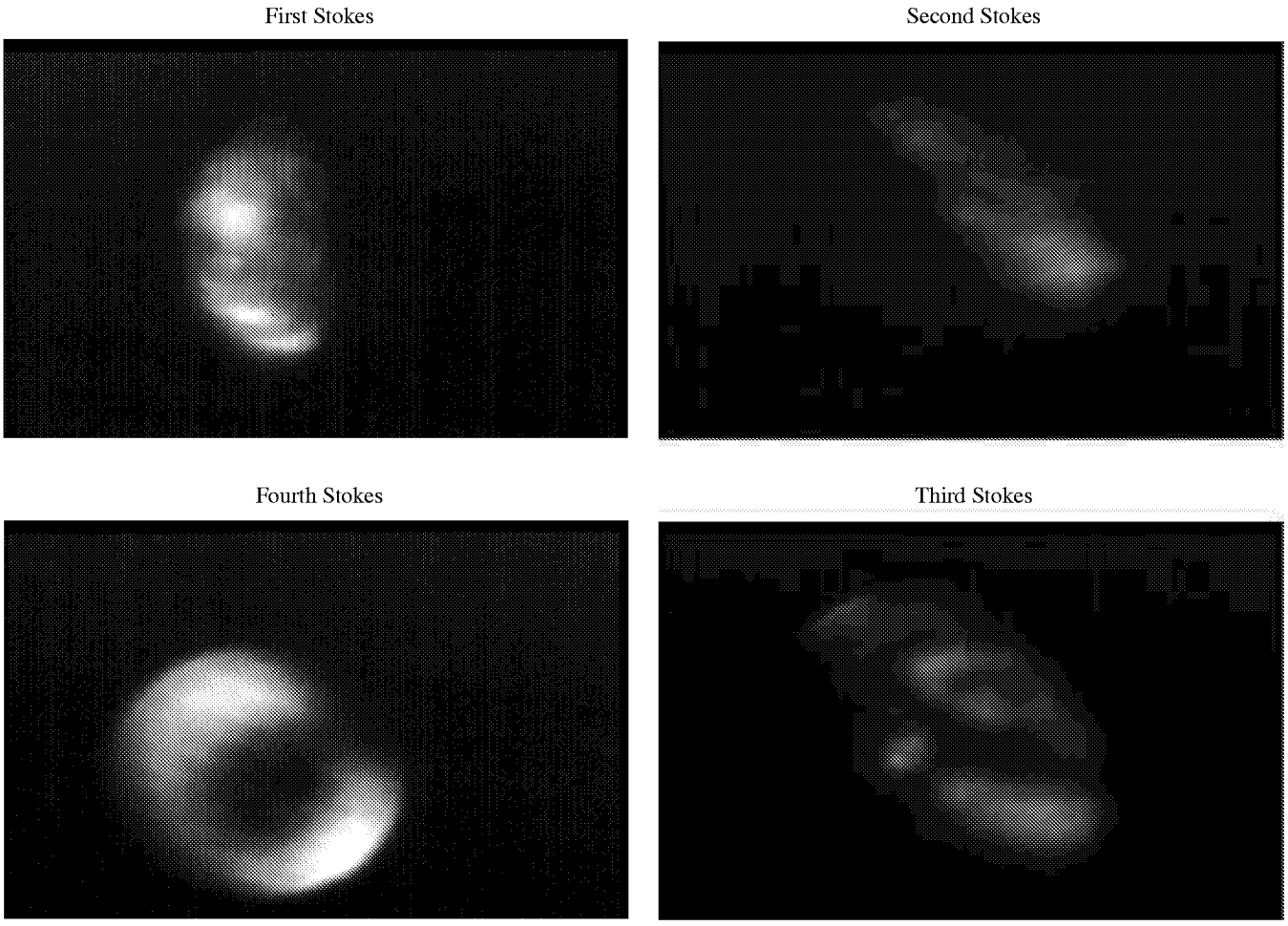

(a) 25-pulse averages of Q_1 through Q_4.

Figure 19. Typical CH_4 pulse intensity profiles.

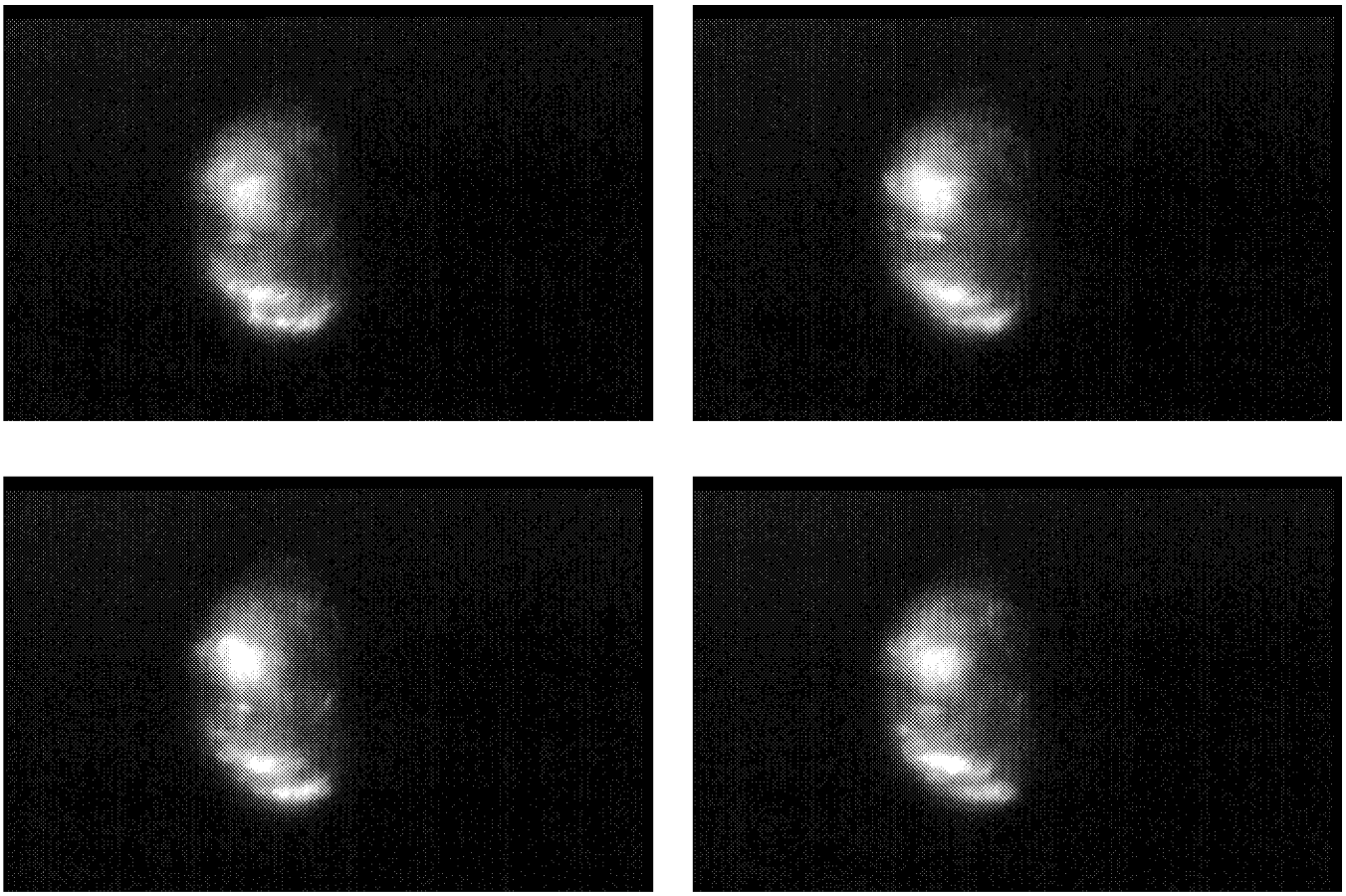

(b) Four single pulse examples of Q_1.

Figure 19. Continued.

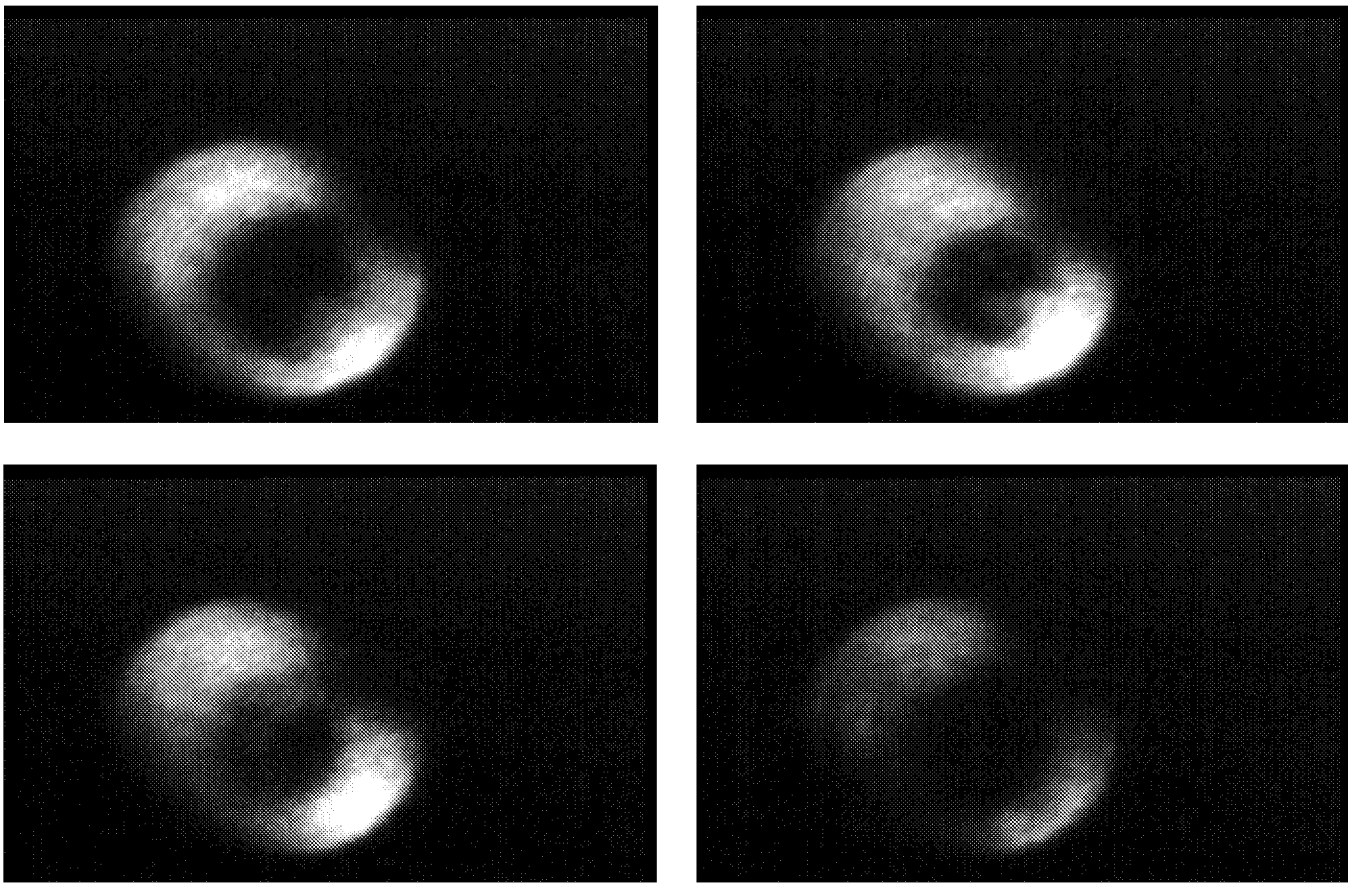

(c) Four single pulse examples of Q_4 doughnut profile.

Figure 19. Concluded.

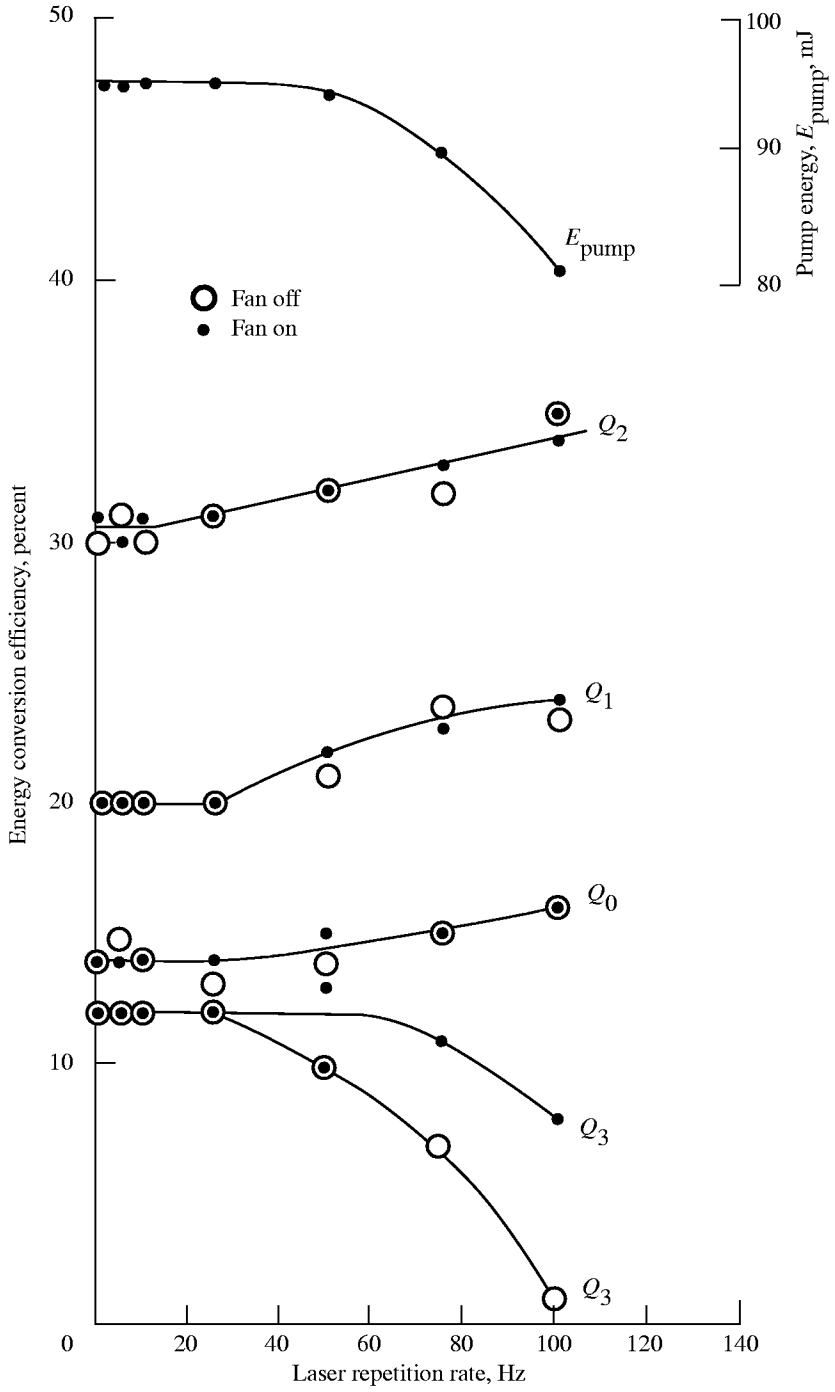

Figure 20. Conversion in 20-amagat H_2 versus repetition rate. Input pump energy (E_{pump}) is read from right-hand scale.

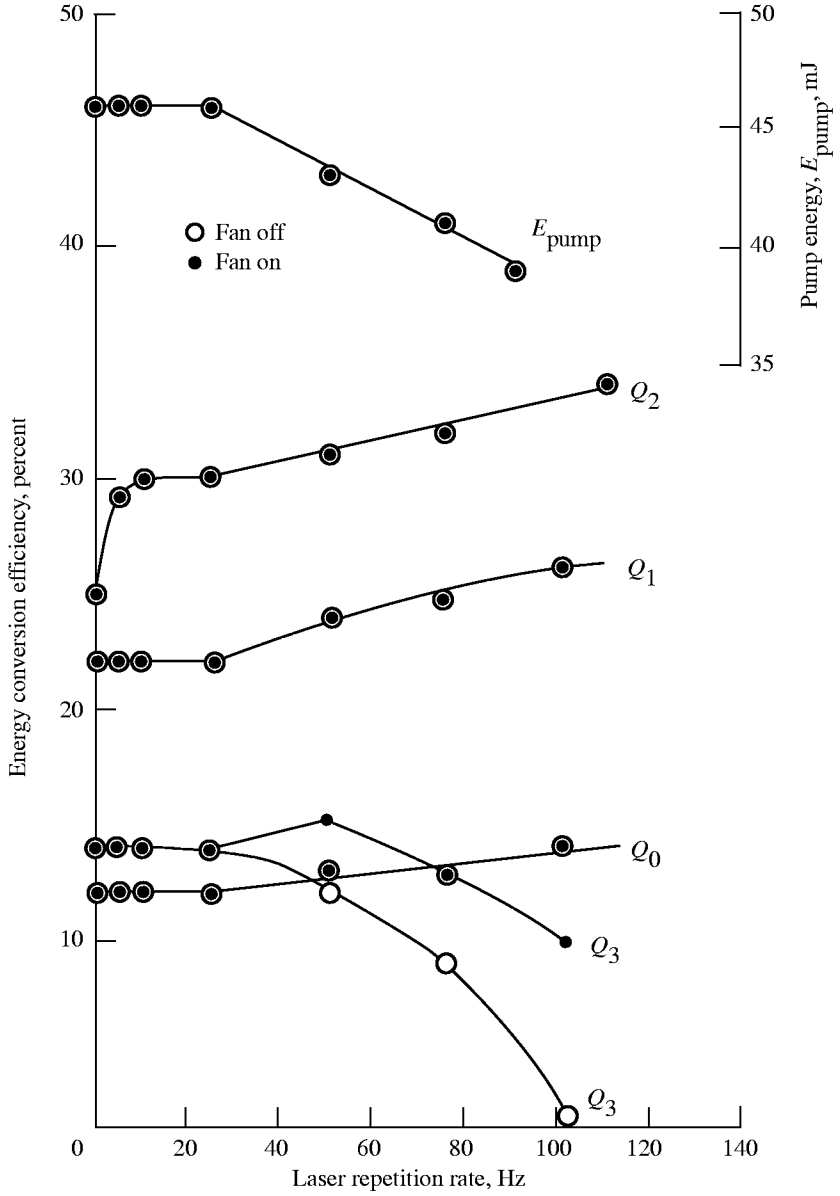

Figure 21. Conversion in 20-amagat H_2.

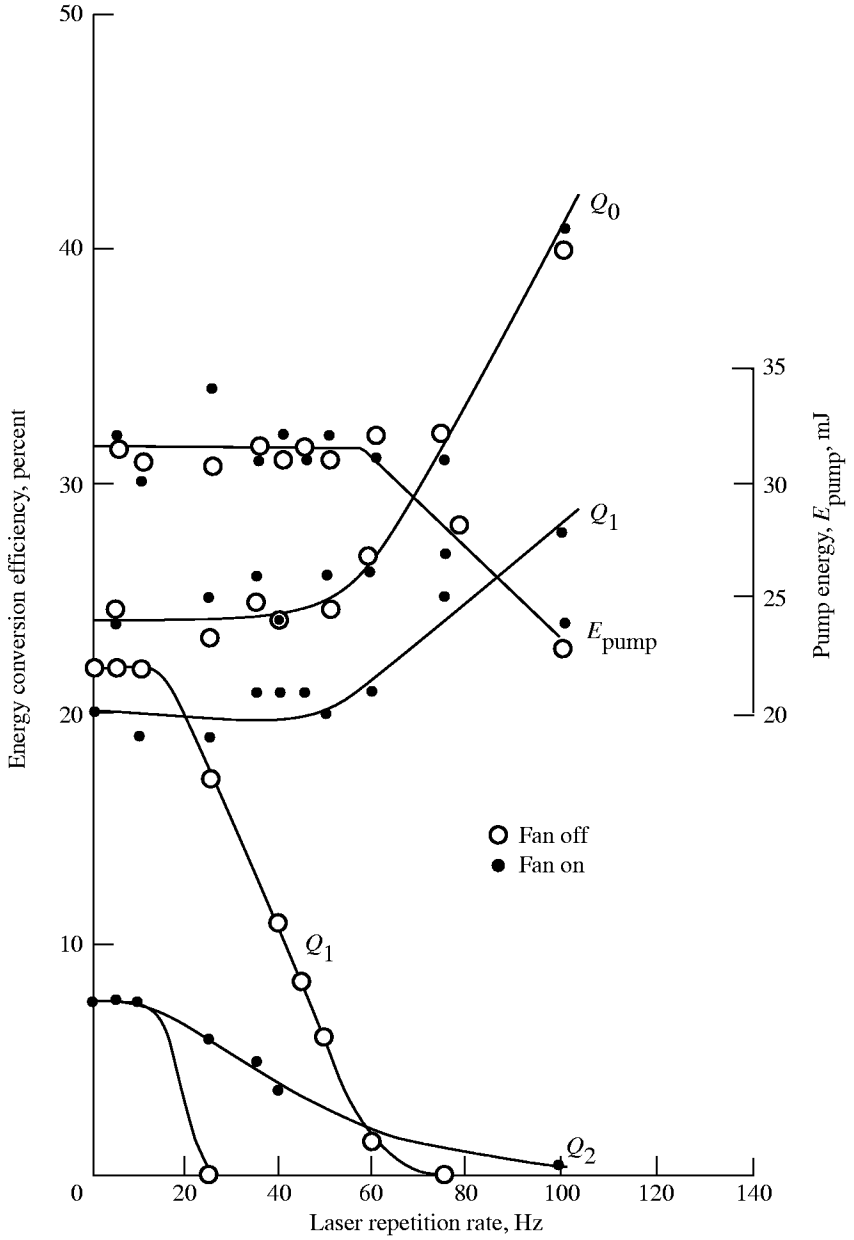

Figure 22. Conversion in 7.2-amagat CH_4 versus repetition rate. To minimize photochemical decomposition, the CH_4 flow rate is 6 SLM.

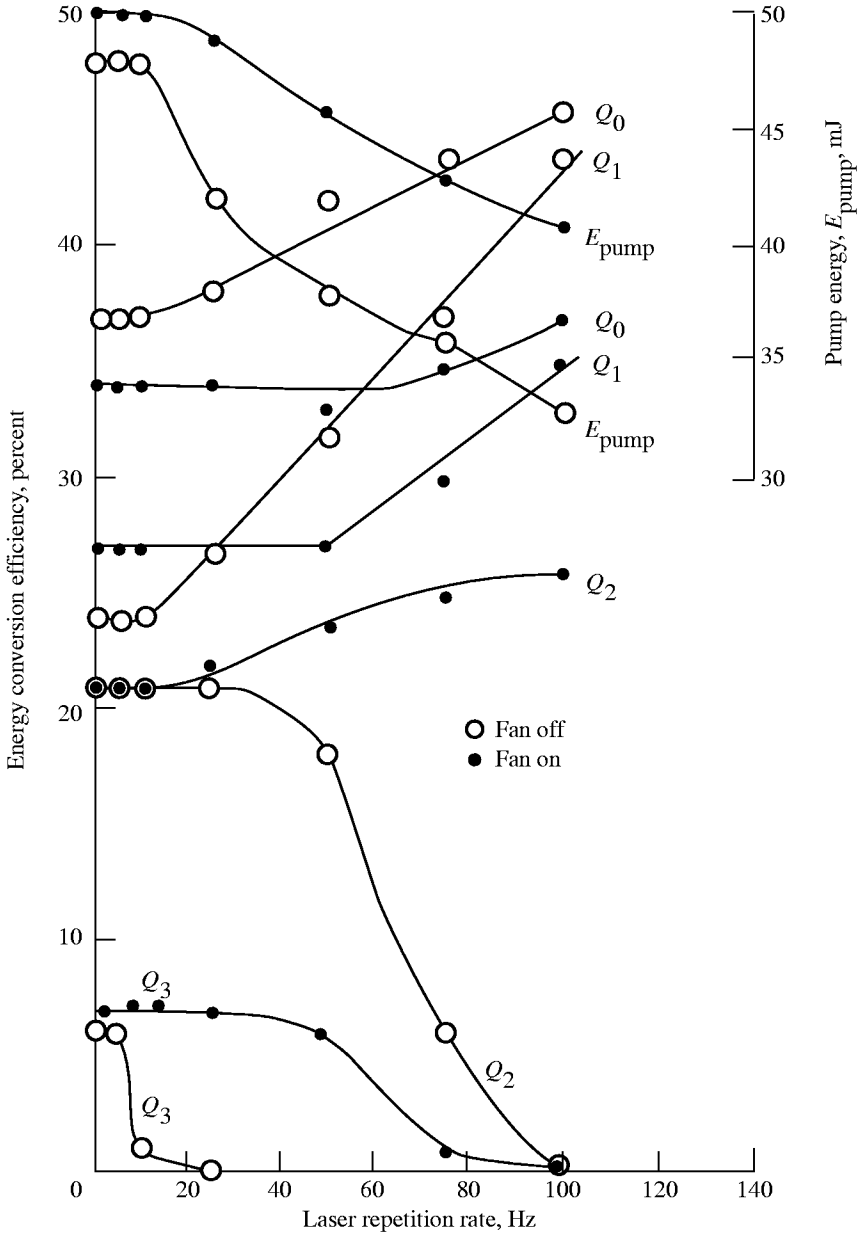

Figure 23. Conversion in 26-amagat D_2 versus repetition rate.

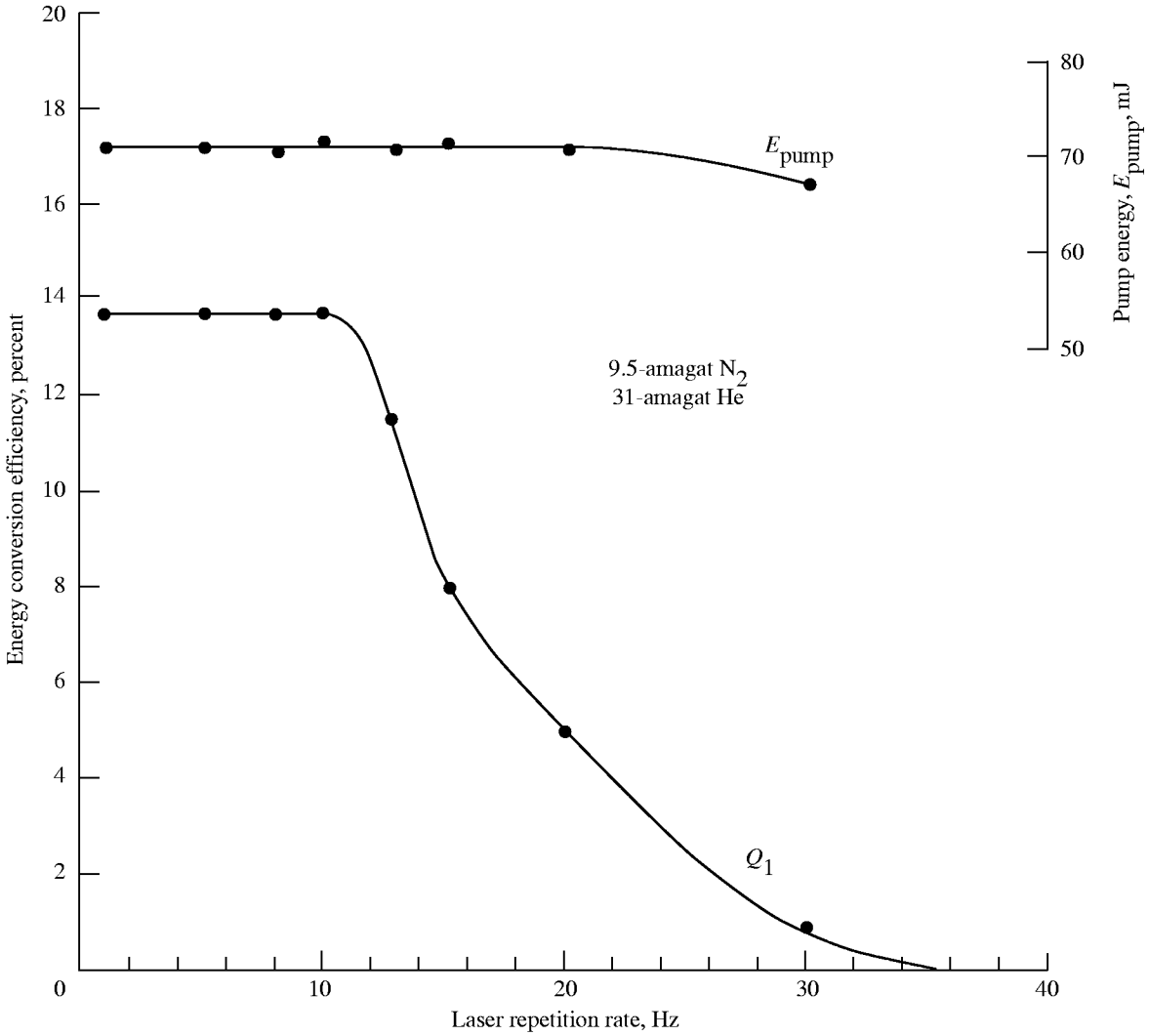

Figure 24. Conversion in 3:1 N_2-He mixture (total density is 126 amagats) versus repetition rate. Input pump energy, 71 mJ; Q_0 constant over range of 1 to 30 Hz.

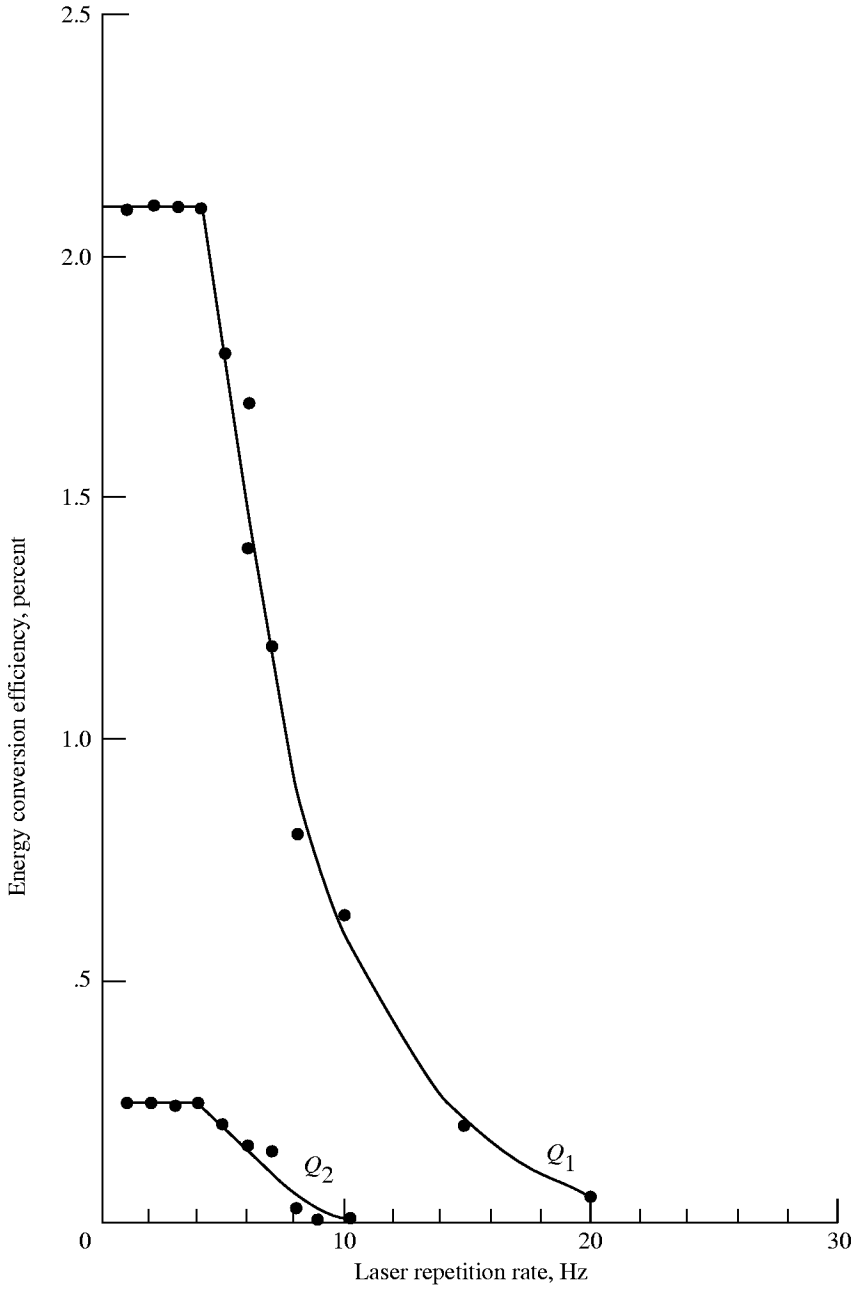

Figure 25. Conversion in mixture of 18-amagat SF_6 and 12-amagat He versus repetition rate. Fan on; input pump energy, 59 mJ; Q_0 constant over range of 1 to 20 Hz.

REPORT DOCUMENTATION PAGE

Form Approved
OMB No. 0704-0188

1. AGENCY USE ONLY *(Leave blank)*	2. REPORT DATE	3. REPORT TYPE AND DATES COVERED
	April 2000	Technical Memorandum

4. TITLE AND SUBTITLE
Raman Shifting a Tunable ArF Excimer Laser to Wavelengths of 190 to 240 nm With a Forced Convection Raman Cell

5. FUNDING NUMBERS
WU 522-31-61-01

6. AUTHOR(S)
R. Jeffrey Balla and G. C. Herring

7. PERFORMING ORGANIZATION NAME(S) AND ADDRESS(ES)
NASA Langley Research Center
Hampton, VA 23681-2199

8. PERFORMING ORGANIZATION REPORT NUMBER
L-17909

9. SPONSORING/MONITORING AGENCY NAME(S) AND ADDRESS(ES)
National Aeronautics and Space Administration
Washington, DC 20546-0001

10. SPONSORING/MONITORING AGENCY REPORT NUMBER
NASA/TM-2000-209710

11. SUPPLEMENTARY NOTES

12a. DISTRIBUTION/AVAILABILITY STATEMENT
Unclassified–Unlimited
Subject Category 74 Distribution: Standard
Availability: NASA CASI (301) 621-0390

12b. DISTRIBUTION CODE

13. ABSTRACT ***(Maximum 200 words)***

Tunable radiation, at ultraviolet wavelengths, is produced by Raman shifting a modified 285-mJ ArF excimer laser. Multiple Stokes outputs are observed in H_2, CH_4, D_2, N_2, SF_6, and CF_4 (20, 22, 53, 21, 2.1, and 0.35 percent, respectively). Numbers in parentheses are the first Stokes energy conversion efficiencies. We can access 70 percent of the frequency range 42000–52000 cm^{-1} (190–240 nm) with Stokes energies that vary from 0.2 μJ to 58 mJ inside the Raman cell. By using 110 mJ of pump energy and D_2, the tunable first Stokes energy varies over the 29–58 mJ range as the wavelength is tuned over the 204–206 nm range. Dependence on input energy, gas pressure, He mixture fraction, and circulation of the gas in the forced convection Raman cell is discussed; Stokes conversion is also discussed for laser repetition rates from 1 to 100 Hz. An empirical equation is given to determine whether forced convection can improve outputs for a given repetition rate.

14. SUBJECT TERMS	15. NUMBER OF PAGES
Raman shifting; Stimulated Raman scattering; Wavelength conversion; Far ultraviolet wavelengths; ArF excimer	54
	16. PRICE CODE A04

17. SECURITY CLASSIFICATION OF REPORT	18. SECURITY CLASSIFICATION OF THIS PAGE	19. SECURITY CLASSIFICATION OF ABSTRACT	20. LIMITATION OF ABSTRACT
Unclassified	Unclassified	Unclassified	UL